MULTI-OBJECTIVE OPTIMIZATION BASED IMAGE SEGMENTATION: METHOD AND APPLICATIONS

KARTHIK RAJA PERIASAMY

B.Tech(Hons.), National Institute of Technology, Durgapur, India

A THESIS SUBMITTED

FOR THE DEGREE OF MASTER OF ENGINEERING

DEPARTMENT OF CHEMICAL & BIOMOLECULAR ENGINEERING

NATIONAL UNIVERSITY OF SINGAPORE

2012

ACKNOWLEDGMENTS

I would like to start with thanking my supervisor Prof. Laksh for his support and guidance during my term at NUS. Whenever I have lost sight of my goal, he has always guided me back to the trail. I have always been a great admirer of his work ethic and his dedication towards teaching. I have enjoyed some long chats with him (related to topics other than research) and am taking inspiration from that for my career after NUS. I also want to thank him for giving me an opportunity to tutor some of his modules which has completely changed my outlook towards teachers.

I would also like to extend my gratitude to Prof. Rangaiah for giving me an opportunity to tutor in CN3421, Dr. Zhou Ying for willingly sharing the crystallization process images to allow me to understand the real images and Dr. Ranga for giving me the breast cancer ultrasound images from IIUM Breast Centre for analysis. I am thankful to Prof. Q. G. Wang and Prof. Min-Sen Chiu for agreeing to examine my thesis. Prof. Natarajan also deserves a special mention for giving me an opportunity to interact with people to get an insight in the food and beverage industry. I am also grateful to Ms. Samantha, Mr. Rajamohan and other departmental staff for their willingness to help out with any problems regarding computer and other facilities immediately without any hassles.

I am glad to have been a part of Informatics and Process Control Unit (IPCU). I have been lucky to have had an opportunity to work with my group mates who have willingly spent time to help me solve my problems and I take this opportunity to acknowledge them for their contributions in my work.

I am always grateful to my family for their hope and belief in me and their financial support. I am indebted to my friends, who have played a huge role in my life. I have some great friends from all over the world who have supported me till

this time and I hope I can hold onto them forever. I would always cherish the times I have spent with them.

I would also like to thank NUS for giving me an opportunity to conduct research and pursue my masters at Singapore.

Last but not the least, I am thankful to God for everything. I always find solace in praying and the God has always played a part in my life.

TABLE OF CONTENTS

SUMMARY

Image analysis plays a crucial role in various fields such as biology, medicine, remote sensing, robotics and manufacturing. Image segmentation is a critical step in image analysis since the result of segmentation plays an important role in feature extraction. In this work, image segmentation is carried out by thresholding. Generally, the threshold is selected by optimizing a single objective. Thresholding can be improved by combining the objectives of two different methods (Otsu and minimum error thresholding methods). Hence, in this work, the optimum threshold is calculated by solving a multi-objective optimization (MOO) problem. The two objectives used in this work are maximizing the between-class variance and the minimizing the error while histogram fitting. This MOO is solved using the plain aggregating approach and simulated annealing by assigning appropriate weights to each objective function. The MOO based thresholding overcomes the limitations of the individual approaches and outperforms the results obtained by thresholding using either of the single objectives. The misclassification rate of the MOO approach is compared with the traditional Otsu and minimum error thresholding methods. The MOO based approach is tested on several examples. The first application is in the estimation of crystal size distribution (CSD) using Particle Vision and Measurement (PVM) images to assist in crystallization process control. In this study, the segmentation results of the developed method are compared with the results of Otsu and minimum error method. The segmented images are further processed by means of feature extraction to estimate the CSD. The algorithm is tested on a set of artificially generated crystallization images. The accuracy of this algorithm is gauged by comparing the CSD estimated to the data used to generate the artificial images. This accuracy was found to be around 92% for images in which about 20

- 25 particles exist. The effect of parameters such as the number of images, the number of particles in the images, and noise level in the images on the estimated CSD is investigated. The second application relates to classifying benign and malignant tumors to assist radiologists involved in the treatment of cancer patients. Our proposed MOO methodology is used to segment the tumors (regions of interest) and the results are compared with the other methods. With the help of feature extraction, a set of required features are extracted from the images. These features can then be used by radiologists for classification purposes and subsequent treatment. In addition to the two abovementioned process and medical applications, other illustrative examples are also included to illuminate the utility of the proposed MOO based thresholding in aiding decision making for real-world applications.

LIST OF TABLES

LIST OF FIGURES

ABBREVIATIONS

CSD	Crystal size distribution
FBRM	Focus beam reflectance measurement
MRI	Magnetic resonance imaging
MOO	Multi-objective optimization
NSGA	Non-dominated sorting genetic algorithm
PVM	Particle vision and measurement
SA	Simulated annealing
SOO	Single objective optimization

NOMENCLATURE

a	Grey level range of the first Gaussian curve
b	Grey level range of the second Gaussian curve
f_l	Focal length of the camera
$f_i(x)$	i^{th} objective function
$f(l)$	Estimated crystal size distribution
$f(s)$	Energy of the current state
$f(s_0)$	Energy of initial state
$h(g)$	Normalized distribution of the image histogram where g denotes the grey level
i	Grey level
j	Number of objectives
k	Boltzmann constant
l	Characteristic length of each particle in the given volume
n	Number of particles captured in the image
n_i	Number of pixels at each grey level
p_i	Normalized probability distribution of the image histogram
s	Current state
s_0	Initial state
t	Temperature of the current state in simulated annealing algorithm
w_i	Weight parameter
x	Solution vector
x_i, y_i	Coordinates on the image plane
$F(t)$	Total objective function

GL	Grey level values of each pixel in an image
$J(T)$	Second objective function
L	Number of grey levels in the image
N	Total number of pixels
$P_i(T)$	Probability distribution of the i^{th} Gaussian curve
V	Imaging volume captured by the camera
S	Search space
T	Optimal threshold
X, Y, Z	Physical coordinates
α	Cooling rate
δE	Change in energy
$\mu_i(T)$	Mean of the i^{th} Gaussian curve
$\mu(k)$	First-order cumulative moments of the histogram up to k^{th} grey level
μ_T	Total mean grey level of the image
${\sigma^2}_B(k)$	Inter-class variance (between class variance) - first objective function
${\sigma^2}_i(T)$	Variance of the i^{th} Gaussian curve
$\omega(k)$	Zeroth-order cumulative moments of the histogram up to k^{th} grey level

Chapter 1

INTRODUCTION

The proverb 'A picture is worth a thousand words' says it all. Perhaps a picture is worth several thousand data samples for it can best reflect the actual state of some processes. With the advent of modern technology, images can be analyzed to achieve certain goals. The main purpose of image processing is to improve the pictorial information and extract information suitable for computer analysis for decision-making and strategic interventions. Image analysis plays a crucial role in extracting meaningful and actionable information from process images. Human eye and the brain together is the best example of an image analysis system. Computer based image analysis can be used to replace human effort so as to make the image analysis process much more fast, efficient and automatic. Various fields such as biology, medicine, remote sensing, robotics and manufacturing benefit from image analysis.

1.1 Motivation

Image analysis has many applications in the chemical, food and pharmaceutical industries spanning areas such as quality control, process control, machine control and robot control. In the food industry, ensuring uniform shape, texture and size of the final products is of paramount importance. Similarly in crystallization processes, it is vital to obtain a desired Crystal Size Distribution (CSD) (Braatz 2002). CSD needs to be estimated at regular intervals for controlling the process effectively. There are many offline technologies such as microscopy for estimating CSD and therby assisting in process control. However, recently the use of in-line

measurements such as Particle Vision and Measurement (PVM) are being explored for estimating CSD (Zhou et al. 2009). PVM can be used to obtain images at any point of time from which the CSD can be estimated. Therefore, image analysis can play a major role in crystallization process control as well.

Medical image analysis involves the analysis of clinical images taken with a view to detect and diagnose diseases associated with body organs or to study the normal physiological processes. These analyses can be performed on images obtained from different imaging technologies such as ultrasound, radiology, magnetic resonance imaging (MRI), etc. Image analysis methodology plays a vital role in cancer diagnosis (Cheng et al. 2010), thereby allowing doctors to decide on the right treatment for the patient. Breast cancer is one of the leading causes of death among women. Generally, while diagnosing and classifying breast cancer images, there are a lot of variables like tumor size, shape, homogeneity, etc. that are taken into account by the physician. Computer based image analysis algorithms can be developed to assist radiologists in classifying tumor images.

1.2 Background

The major steps involved in image processing are shown in Fig. 1.1 (Jain 2001, Gonzalez & Woods 2008, Dougherty 2009).

The purpose of each step is described briefly:

1. Image acquisition: to acquire a digital image.

2. Image pre-processing: to improve the image suitable for analysis.

3. Image segmentation: to partition an image into multiple regions and to extract the region of interest from the remaining.

4. Feature extraction: to convert an input image to a set of features based on the attributes of segmented image.

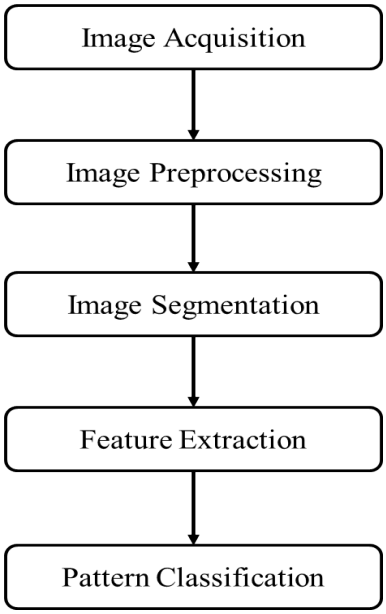

Fig. 1.1. Steps in image analysis

5. Pattern classification: to classify the given input image based on extracted features.

Image pre-processing involves techniques such as noise reduction, contrast enhancement and image sharpening where both input and output are images. In image segmentation, regions of interest are extracted from the image. Usually, in feature extraction and pattern classification, the inputs are images and the outputs are data (like features of segmented objects) obtained from the images. Different techniques are used to perform each step in image analysis based on the intended application. Hence, the technique selected at each step is very important to obtain the desired result from the algorithm.

1.3 Objectives

The main objective of this work is to apply image analysis to solve problems that are of interest to industry and medicine. The novelty in this thesis is that an MOO based thresholding approach has been applied to problems such as segmentation of

crystals from process images and extraction of tumor portions from breast ultrasound images. This thesis shows that the proposed MOO based approach improves the segmentation quality compared to those obtained using some available single objectives.

The main objective will be accomplished through the following sub-objectives:

1. Developing a method which selects a suitable threshold for image segmentation based on multi-objective optimization (MOO) and comparing its results with a few common thresholding methods.

2. Designing an image analysis algorithm that can estimate CSD from PVM images and validating this algorithm using a library of artificial images generated based on certain assumptions.

3. Designing an image analysis algorithm that can assist radiologists in classifying breast ultrasound images into benign and malignant tumors.

1.4 Organization of the Thesis

The reminder of this thesis is organized into four chapters as follows:

- Chapter 2: Definitions of the terminologies and review of the techniques used in this thesis are given.

- Chapter 3: Image segmentation based on multi-objective optimization is explained along with examples and the results are compared with those obtained from other segmentation methods.

- Chapter 4: Image analysis techniques are applied to two case studies: crystallization process images and breast cancer ultrasound images.

- Chapter 5: The conclusions obtained from this thesis work along with recommendations for possible future research work are provided.

Chapter 2

DEFINITIONS AND DEVELOPMENTS IN IMAGE ANALYSIS

Image analysis is a very important tool in today's world. To understand the developments in image analysis, one must be familiar with some basic definitions related to the image analysis domain.

An image is generally a visual representation of some object. An image can be a photograph captured by an optical device such as a camera or a drawing rendered manually from the information captured or imagined by the human brain through the eye.

2.1 Digital Image

An image in the real world is defined as a function of two variables $a(x, y)$ where a is the amplitude assigned to any coordinate position (x, y) (Gonzalez & Woods 2008). A digital image described in a $2D$ discrete space is derived from a continuous image $a(x, y)$ through a sampling process that is referred to as digitization (Young et al. 1995).

The digitization is done by dividing the continuous image into P rows and Q columns. The intersection of a row and a column is referred to as a pixel. An example of a digitized grey scale image is given in Fig. 2.1 [1]. A continuous grey scale image is taken and digitized by dividing into $P = 9$ rows and $Q = 12$ columns. Each pixel is given an intensity value depending on the brightness at that particular

[1]Image Courtesy : MATLAB

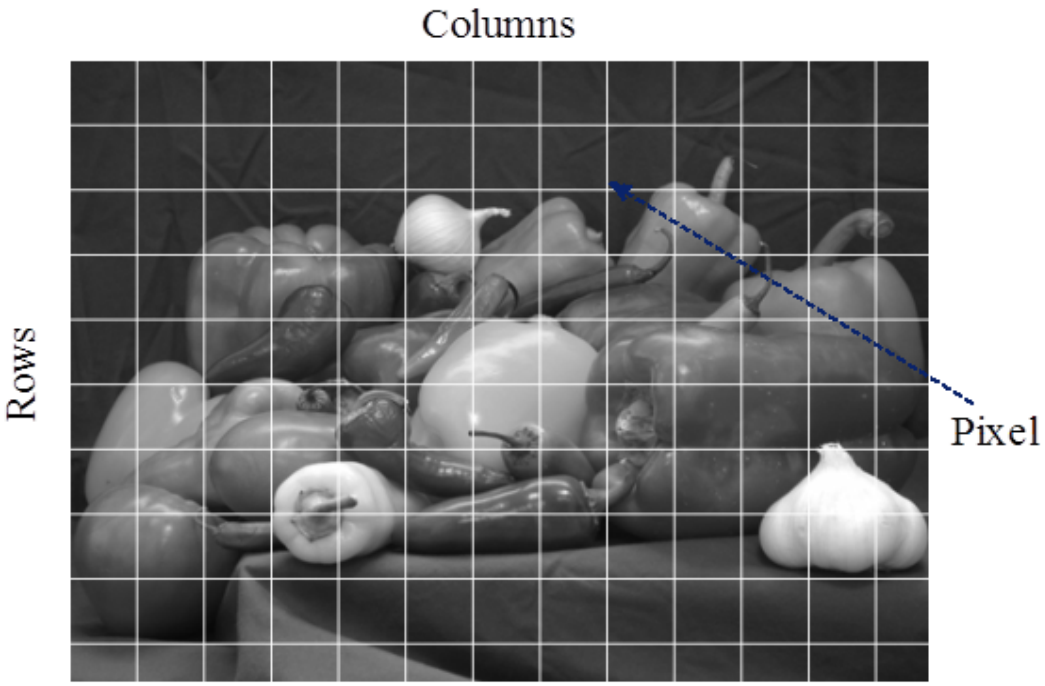

Fig. 2.1. Illustration of a digitized image

point. Generally, a grey scale image has 8 bit color depth which indicates $2^8 = 256$ colors. Hence, grey scale intensity value varies from 0 - 255. This process of assigning intensity values to a pixel is referred to as quantization.

2.2 Image operations

Image operations are performed on an input digital image to result in an output image based on the user's requirement. Image operators are classified based on its function/effect on the image.

2.2.1 Types of operations

Operations performed on digital images are classified into three categories based on its processing characteristic (Young et al. 1995, Bebis 2004*b*).

The different types of operators are described in Table 2.1 and illustrated in Fig. 2.2.

Table 2.1
Different types of image operations

Operation	Description
Point operation	The output value of the particular pixel is dependent only on the input value at that particular point.
Local operation	The output value of the particular pixel is dependent only on the input value in the neighborhood at that particular point.
Global operation	The output value of the particular pixel is dependent on the entire image.

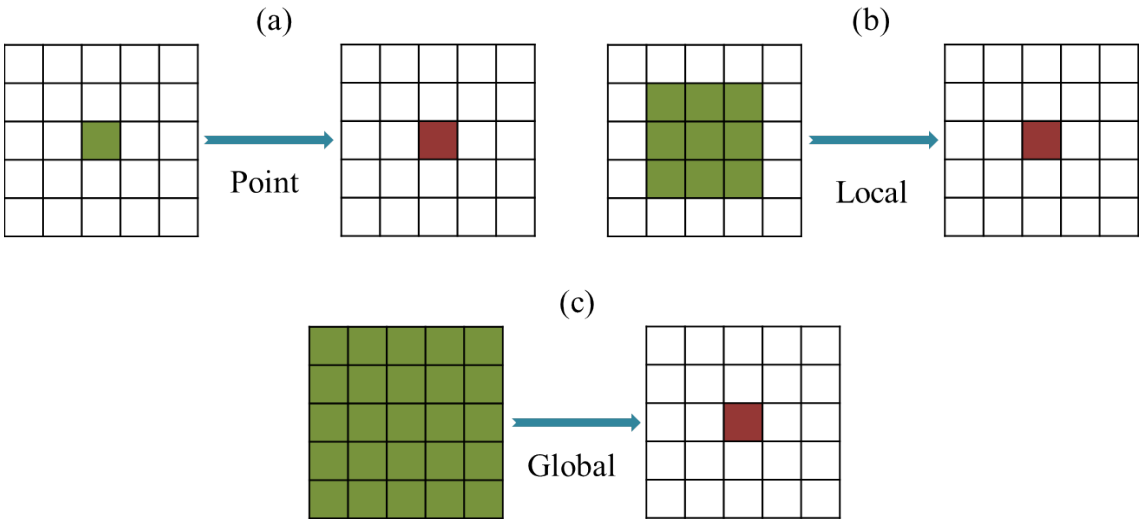

Fig. 2.2. Illustration of different types of image operations

2.2.2 Image neighborhood

While performing local operations, a neighborhood of connected pixels is taken into consideration. Different types of connectivity are used in defining different types

of neighborhood (Young et al. 1995). Since we are dealing only with rectangular sampling (images are digitized by laying a rectangular grid over the continuous image), only the related types of neighborhood are explained in Table 2.2.

Table 2.2
Different types of neighborhood

Neighborhood	Connectivity	Description
Von Neumann neighborhood	4-connected	Pixels that touches the edges of the pixel.
Moore neighborhood	8-connected	Pixels that touches the edges and corners of the pixel

The different types of neighborhood are also illustrated in Fig. 2.3.

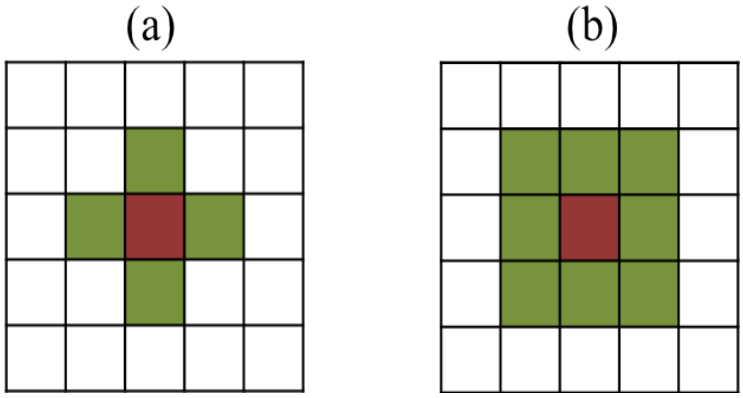

Fig. 2.3. (a) 4-connected neighborhood and (b) 8-connected neighborhood

2.3 Image histogram

An image histogram is used to plot the frequency distribution of grey level intensities in an image (Gonzalez & Woods 2008). Fig. 2.4 shows the histogram of the image given in Fig. 2.1. It provides a summary of the intensity level in the image. Image histogram can be used to obtain the significant range of the grey level

intensities of the image. In Fig. 2.4, the height of the curve denotes the number of pixels with the given grey level intensity.

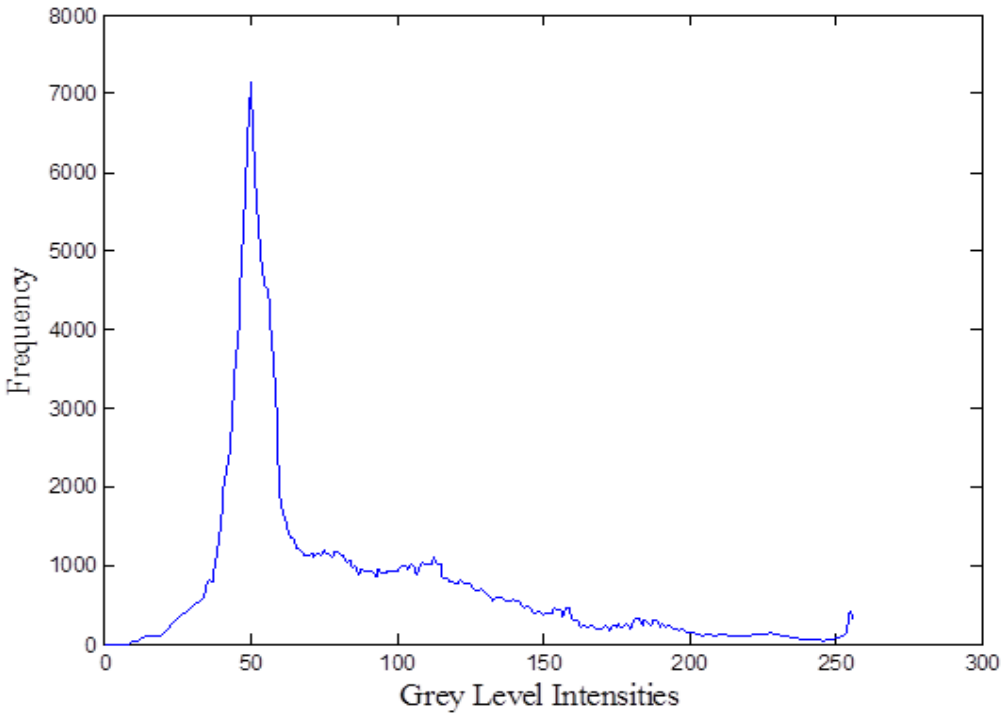

Fig. 2.4. Image histogram

2.4 Image analysis

Next, the major steps involved in image analysis are explained along with the techniques that are used in this work.

2.4.1 Image acquisition

Image acquisition is the process of acquiring a real world image and storing it in a format (digital image) that can be processed by a computer algorithm (Gonzalez & Woods 2008). During this acquisition process, a lot of noise may become embedded in the image posing challenges for the image analysis algorithm.

Noise is defined as random changes introduced into the image due to disturbances from the environment (Boncelet 2005, Gonzalez & Woods 2008). Noise in the images can originate due to the sensitivity of camera to light and/or during data transfer and storage (file formats). Sources of disturbances during image capturing can be light, equipment error, human error, etc. Disturbances in data storage can be caused due to file conversion, compression, transfer, etc. At each step, the disturbances can cause different types of noise. Most noises can be modeled into one of the following three types.

Additive Gaussian noise is the simplest form of noise. This type of noise can be described as adding a noise to the image to create a noisy image. Hence, this type of noise is independent of the pixel value in the image. This noise model is assumed to follows a Gaussian distribution (Jain 2001). Equation 2.1 describes the additive noise. The original image is shown in Fig. 2.5(a). Effect of the Gaussian noise on the original image is shown in Fig. 2.5(b).

$$Noisy\ Image = Image + Noise\ Model \tag{2.1}$$

Camera sensors are prone to cause noise because of their inability to differentiate between the photoelectric effect electrons generated by the heat produced in the system and the electrons generated by the actual signal (Gino 2004). The effect of this type of noise is generally proportional to the input signal. Hence, the noise is assumed to be multiplicative in nature. This type of noise is known as *speckle noise*. This noise model is encountered in many images. Denoising speckle noises are quite tricky since it is directly associated with the pixel value (Jain 2001). This can be seen in the noisy image shown in Fig. 2.5(c).

Errors in data transmission can cause black and white pixels randomly throughout the image, commonly known as *impulse noise*. Impulse noise is also known as salt and pepper noise. This type of noise has the property of changing a random pixel to either maximum or minimum value. Hence, an image affected with impulse

noise has black or white dots spread over the image (salt and pepper effect). Black and white dots are visible in the image shown in Fig. 2.5(d).

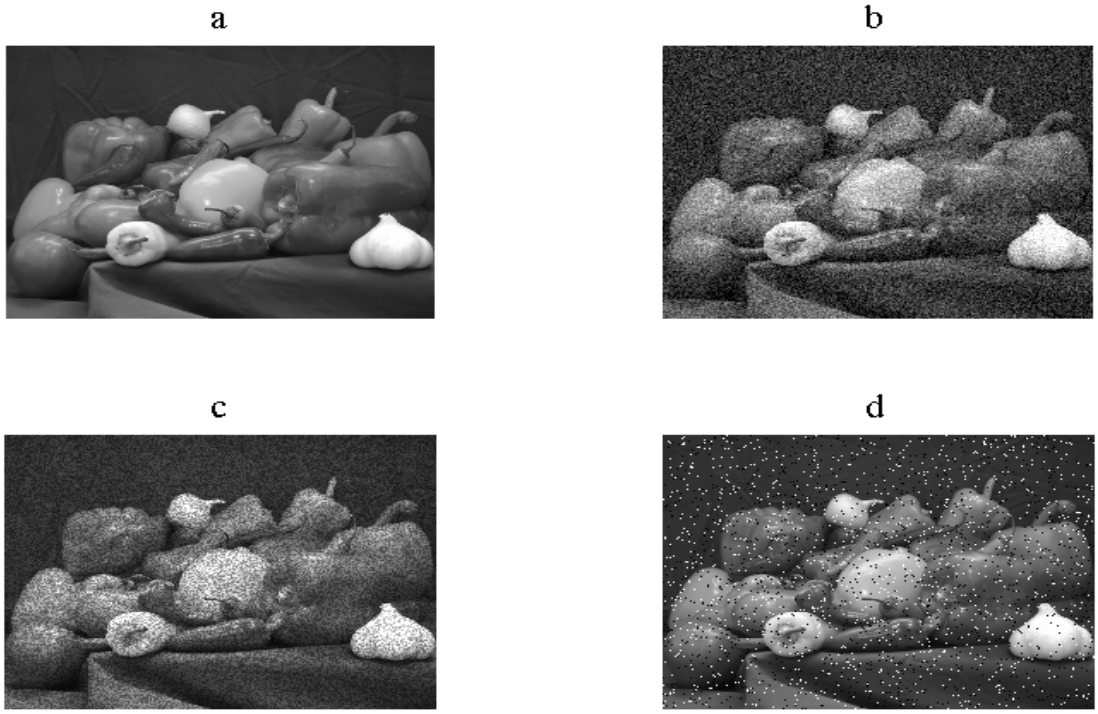

Fig. 2.5. Effects of different noises on an image

Other than this, there are other models used to describe noise - quantization, uniform noise and photon counting noise are mentioned in the literature.

2.4.2 Image pre-processing

Image pre-processing is carried out to convert the raw image into a suitable image for analysis (Jain 2001). This step is characterized by noise removal and image enhancement. Filtering techniques are commonly used for noise removal. Different filtering techniques are used to address different types of noises (Gonzalez et al. 2011). Filters can be classified as linear and non-linear filters. Mean filter is an example of linear filter. This type of filter performs the averaging operation on

each pixel in the image within a neighborhood. The most commonly used non-linear filter is the median filter. Median filter is used to remove distinct odd noises in the image. In this type of filter, each pixel value in the image is replaced by the median value of the neighborhood. An example of mean and median filter is shown in Fig. 2.6. The focus in this figure is on the denoising of the pixel at the centre.

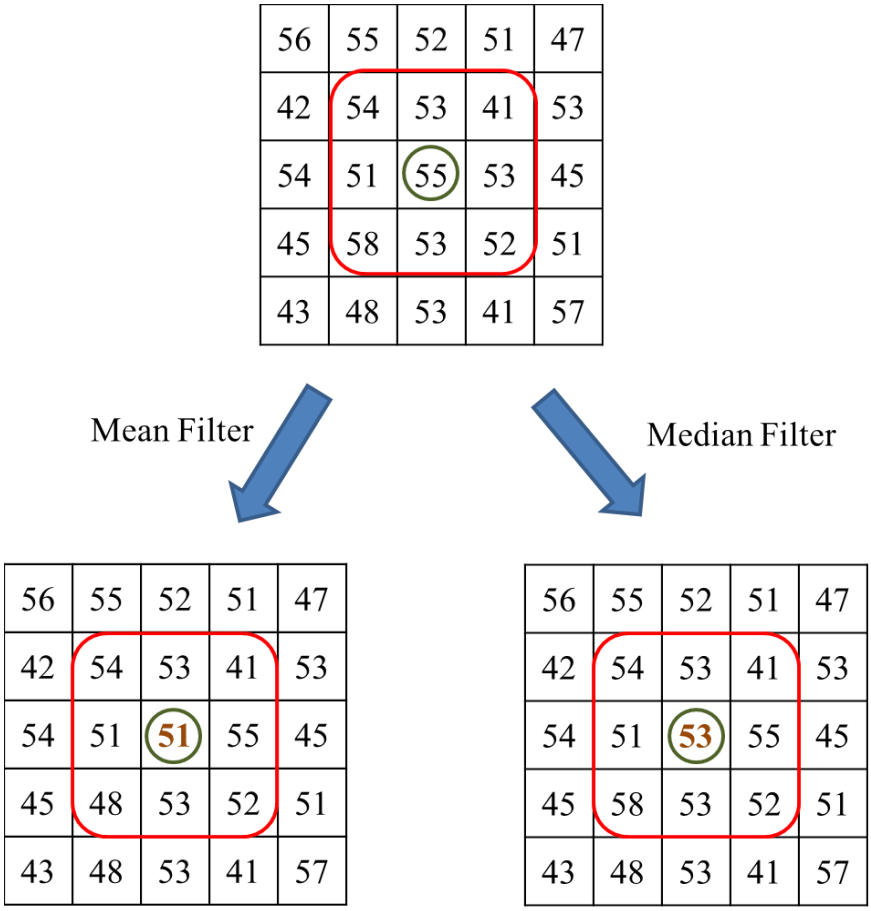

Fig. 2.6. Filtering technique

Image enhancement improves the quality of the image by adjusting the contrast of the image. A few commonly used methods are contrast stretching, histogram equalization, etc. In contrast stretching technique, the total contrast of the image is increased. In general, this method is used to convert a narrow range of grey level intensity values into a wider range. This is done by mapping the intensity values of the original image into new values by stretching the lower and upper bound to 0

and 255, respectively (Gonzalez et al. 2011). In histogram equalization technique, the image is transformed such that the image has a desired histogram (Fisher 1997). This technique is very effective in detailed enhancement and removal of non-linear errors caused by digitizers.

2.4.3 Image segmentation

Image segmentation is a vital step in image analysis. The objective of image segmentation is to partition an image into several regions (Gonzalez & Woods 2008). Image segmentation algorithms are based on two properties of intensity values namely discontinuities and similarities. Methods based on discontinuities in intensity values identify the images using abrupt changes (edge detection) in intensity values. In the second method, groups of pixels of similar values (homogeneous regions) are combined together as one class. Techniques such as thresholding and region growing algorithms fall in this category. The technique used for segmentation largely depends on the type of image used and the intended application of the segmented object. Thresholding is simple and easy to implement segmentation technique. In this technique, a suitable threshold is selected so that the pixels above the threshold are classified into one class and the pixels below the threshold are classified into another class. This type of image is known as binary image. A binary image is defined as an image where the pixel has a value of 0 or 1. Selecting an optimal threshold is a key challenge faced in the threshold based segmentation technique. There are many different methods used to select a suitable threshold (Sahoo et al. 1988, Glasbey 1993). Thresholding methods can be broadly classified into six major categories (Sezgin & Sankur 2004). The categories are explained below:

Histogram shape-based methods: Here, the threshold selection is based on peaks and valleys of the histogram.

Clustering-based methods: In this method, the grey level intensities are clustered into two groups namely background and object.

Entropy based methods: This method uses the entropies of the object, background and the image to calculate the threshold.

Object attribute based methods: Here, the threshold is obtained based on the similarity between the binarized and the original grey level image.

Spatial methods: The threshold is calculated using correlations between pixels.

Local method: In this method, an adaptive threshold is found at each pixel based on local image characteristics.

After image segmentation, morphological operations are applied on the binary images. Morphological operations are performed to change the structure of the objects based on the information required (Fisher 1997, Smith 1997). They are used for representation of image shapes. There are two fundamental morphological image operations known as dilation and erosion. Erosion operation removes the boundary particles and hence, the skeleton of the object is obtained. In dilation operation, the object grows or thickens. The boundary of the objects enlarges to allow the edges to be continuous. This step increases the areas of the object, reducing the size of the holes. This operation also has the ability to remove small unwanted objects such as noise, broken chips, particles touching the border etc.

2.4.4 Feature extraction and classification

Feature extraction is a dimensionality reduction technique. This step is used to reduce the higher dimensional input data into an output (features) of lower dimension. In this work, it is used to extract the characteristics of the segmented objects (Haralick et al. 1973, Choraś 2007). The features extracted can be classified into different types: texture, shape, color and other basic properties of the object. Some common features used are:

Texture based features: entropy, energy, mean of grey level intensities.

Shape based features: descriptors, blob detection.

The extracted features can be used to classify the region of interest with the help of a suitable classifier. This step is known as pattern classification. In this step, classification tools assign segmented objects to different classes based on their features. Some commonly used classification tools are based on multivariate statistical methods, neural networks, artificial intelligence based techniques such as decision trees, etc (Jain et al. 2000, Niuniu & Yuxun 2010).

As mentioned earlier, image analysis has and is increasingly used to solve problems in industrial, environmental and biomedical domains. Below, we describe two application areas that this thesis work will focus upon.

2.5 Image analysis in crystallization

Crystallization is one of the basic unit operations employed in the pharmaceutical industries. The size, shape and purity of the crystal influence further downstream processing. Hence, it is critical to control the crystallization process. It must be noted that control of crystallization process is made more challenging because of its high sensitivity to disturbances (Braatz 2002). Crystal Size Distribution (CSD) is one of the important characteristics to be monitored and controlled in order to obtain crystals of desired quality (Larsen, Patience & Rawlings 2006). Techniques such as laser based Focus Beam Reflectance Measurement (FBRM) and Particle Vision and Measurement (PVM) are widely used for online monitoring of the crystallization process.

In FBRM technique, a laser beam is focused using a rotating lens into the crystallizer. The light is scattered when the beam passes through a particle. Based on the duration required for the light to scatter back, the chord length of the particle is measured. The major drawback in the FBRM technique is that the chord length distribution measured is not the actual particle size distribution since the chord length measured randomly may not represent the entire particle. This limitation can be overcome with the use of PVM technique as direct measurement from the

process image is possible (Presles et al. 2010). In PVM technique, the process images are captured either as videos or pictures with the help of a camera; these pictures are analyzed to get direct estimate of CSD (Patience & Rawlings 2001, Zhou et al. 2009).

In crystallization imaging techniques, CSD can be estimated from crystallization images by segmentation, where, crystals are extracted from the background. However, segmentation of the crystal image poses a challenge due to crystal overlaps and disturbances in the system such as agglomeration, breakage and attrition. Once crystals are segmented from the image background, size and shape descriptors are used to characterize possible crystal shapes. These descriptors are used to extract features (properties) such as size, aspect ratio, roundness, etc (Lovette et al. 2008).

2.5.1 Literature on estimation of CSD based on image analysis

Pons and Vivier used offline image analysis to characterize crystal shape and determine its structural parameters (Pons & Vivier 1990). Plummer and Kausch measured CSDs of crystallized polyoxymethylene under a microscope (Plummer & Kausch 1995). Monnier et al. used offline image analysis to estimate CSDs and compared it with in situ laser measurements (Monnier et al. 1997). Puel et al. used image analysis to evaluate shape factors by measuring two characteristic lengths (length and width) (Puel et al. 1997). These shape factors were used to quantify the habit of the crystals. Similar method was used to evaluate shape factors of crystal in batch processes (Puel et al. 2003, Oullion et al. 2007). Korath et al. measured CSD accounting for touching particles as well (Korath et al. 2006, 2007). Zhou et al. combined image processing techniques with statistical multivariate image analysis to characterize shape and size of the crystal (Zhou et al. 2006). Mironescu et al. used fractal analysis to estimate CSD (Mironescu & Mironescu 2006). Larsen et al. developed an image analysis algorithm based on linear features for segmenting needle

shaped particles (high aspect ratio particles) (Larsen, Rawlings & Ferrier 2006). Later, they extended it to be used for other shapes as well (Larsen et al. 2007). Presles et al. developed an algorithm by modifying the watershed segmentation and validated the algorithm through experimental and simulated results (Presles et al. 2010). A summary of methodologies used in the reviewed works along with their main characteristics is given in Table 2.3.

2.6 Image analysis in breast cancer detection

Breast Cancer is the most frequently diagnosed cancer and the leading cause of cancer death among women. Breast cancer accounts for 23% of the total cancer cases and 14% of the total cancer deaths among women (Jemal et al. 2011). The best way to reduce the number of cancer deaths is to diagnose and treat the disease at earlier stages. Therefore, a good reliable approach is required for detection and diagnosing breast cancer. Such an approach should be able to distinguish between benign and malignant tumors with low false positive and false negative rates (Cheng et al. 2010). Mammography is a widely used technique for detecting and diagnosing breast tumors. However, this technique has certain limitations for breast cancer detection. Mammography technique uses X-rays (ionising radiation) for the detection. Detection based on mammography has high rate of false positives resulting in a number of unnecessary biopsies (Fordham 1977, Cheng et al. 2010). Mammography cannot detect breast cancer in women with dense breasts. However, these limitations can be overcome by using ultrasound imaging. Ultrasound technique has an advantage of being a very safe and convenient technique since it does not use radiation. Ultrasound technique also works out to be less expensive compared to mammography. Ultrasound has a very good detection rate in differentiating cysts. Ultrasound based detection does not have trouble imaging in women with dense breasts.

Generally, radiologists diagnose breast cancers by analyzing the ultrasound image for information. However, they are required to be very well trained to detect cancers using ultrasound. Hence, the detection of breast tumor is largely human dependent and is prone to a high inter-observer variation. Therefore, there is a need for computer-aided diagnosis (CAD) to assist radiologists in tumor classification (Hadjiiski et al. 2006).

2.6.1 Literature on breast ultrasound images detection and classification based on image analysis

Chen et al. used local neighborhood statistics based features as the criterion to classify breast tumors (Chen 1999). Horsch et al. developed an efficient algorithm for segmenting potential tumor regions based on their margins (Horsch et al. 2001). Joo et al. used image analysis to identify benign nodules in ultrasound images to avoid unnecessary biopsies (Joo, Moon & Kim 2004, Joo, Yang, Moon & Kim 2004). Chang et al. developed an algorithm which used morphological features to classify breast tumors (Chang et al. 2005). Moon et al. applied the same algorithm with different set of features to continuous ultrasonographic images (Moon et al. 2005). Similarly, a number of works to identify benign tumors from malignant exist in the literature. Song et al. compared two different classification techniques to classify breast sonograms based on shape and margin features (Song et al. 2005). Cheng et al. presented a review on CAD of breast cancer using ultrasound images and compared different techniques with their advantages and disadvantages (Cheng et al. 2010). It is evident from literature that tumor can be segmented from ultrasound images. The features from the segmented tumors can be used for classifying tumor into benign or malignant. The methodologies used in the literature are summarized in Table 2.4.

2.7 Challenges in image analysis

The problems faced in the application of image analysis along with possible ways to overcome them are discussed here.

Image segmentation is a critical step in image analysis since good results from the segmentation step is vital for feature extraction. Therefore, a good segmentation technique has to be used for effective image analysis. In this work, image thresholding is preferred because of its simplicity and easy implementation. Hence, a suitable method has to be chosen to obtain the optimal threshold. The most common methods used for selecting an optimal threshold are mode method, Otsu method, minimum error method and entropy based method. The origins of these methods are explained below.

Mode method is a type of histogram shape based thresholding method. It uses the concept of valley to calculate the threshold. In this method, the threshold is selected as the minimum intensity value in the valley between the two peaks (object and background) (Prewitt & Mendelsohn 1966). Otsu method and minimum error method are clustering based methods. Otsu method uses the variance of the background and object pixels (Otsu 1979). The optimal threshold is obtained by maximizing either the variance between the two classes or minimizing the variance within the same class. Minimum error method assumes two Gaussian distributions to fit the image histogram (Kittler & Illingworth 1986). The two distributions are assumed to correspond to the object and background. The threshold at which the Gaussian distributions fit the actual histogram with minimum error is taken as the optimal threshold. Entropy method uses the entropy of the image to calculate the threshold (Pun 1980, Kapur et al. 1985). The optimal threshold is selected such that the sum of the entropy of the two classes (object and background) reaches its maximum.

These methods work well for ideal images (objects and background with distinct grey level intensities). However, these methods do have limitations while applied to

real world images (Bebis 2004*c*, Sezgin & Sankur 2004). Hence, these methods can be combined in a way so that the weakness of each method can be overcome and better quality information can be extracted from the images. For example, multi-objective optimization can be applied to obtain the optimal threshold by combining the objectives from the two thresholding methods. Some works reported in the literature do use the MOO approach to obtain the optimal threshold. They are listed below.

Nakib et al. used modified within-class variance and overall probability of error as the two objectives and solved the MOO by using weighted sum method and enhanced simulated annealing (Nakib et al. 2007, 2008). Later, they considered modified within-class variance and entropy criterion as the two objectives and solved the MOO using a non-Pareto approach (Nakib et al. 2009*a*,*b*). Xinming and Chunhong used 2D entropy criterion and 2D Otsu method as their objectives and solved it using weighted sum method and simulated annealing (Zhang & Liu 2009). Later, Nakib et al. used biased intraclass variance, Shannon entropy criterion and 2D entropy criterion and solved it using NSGA II (Nakib et al. 2010). These methods have been found to be successful on simple images. However, these methods are yet to be tested in real-world applications.

In this work, an MOO based image thresholding is used. The objective functions used in this work are between-class variance and minimum error. MOO problem is solved using simulated annealing because of its ability to effectively handle combinatorial problems. The developed method is tested on several examples including the estimation of crystal size distribution for crystallization process control and to segment ultrasound images for classifying tumors in breast cancer screening campaigns.

Table 2.3
Developments in image analysis for application in crystallization

Year	Author	Methodology	Remarks
1990	Pons and Vivier	Thresholding Morphological processing Polygonal representation	Offline imaging
1995	Plummer and Kausch	Spatial filter Thresholding Particle detection routine	Offline imaging
2006 2007	Korath et al.	Median filter Otsu thresholding Morphological processing Particle counting technique	Separates touching particles. Error in measurement due to erosion
2006 2009	Zhou Ying et al.	Contrast-limited adaptive histogram equalization Canny edge detector Morphological processing Rotating clipper method Multiway principle component analysis for classification	Error in measurement due to random orientation of particles. Currently applied to square and diamond morphologies
2006	Mironescu et al.	Thresholding Box counting method	Fractal analysis to calculate the dimension
2006	Larsen et al.	Segmentation for High-Aspect-Ratio Crystals (SHARC)	Novel method for needle shaped particles
2007	Larsen et al.	Model-based SHApe Recognition for Crystals (M-SHARC)	Extended the SHARC method for other shapes
2010	Presles et al.	Watershed segmentation method Image Restoration to construct the particle outside the focal plane	Validation through experimental method and computer simulation. Computationally intensive.

Table 2.4
Developments in image analysis for application in breast cancer detection

Year	Author	Methodology	Remarks
1999	Chen et al	Feature extraction - statistics based on local neighborhood Classification - artificial neural networks	This methodology can be used to cross check for physicians. Tested on small datasets
2004	S Joo et al.	Median filtering - filter size (4X4) Thresholding - valley based Morphological image processing Feature extraction - spiculation, ellipsoid shape, brightness, branch pattern and number of lobulations Classification - artificial neural network	This method selects the region of interest manually.
2005	Chang et al	Anisotropic diffusion filtering and stick method Thresholding - level set method Feature extraction - form factor, roundness, aspect ratio, convexity, solidity and extent Classification - support vector machines	Morphological features used to overcome the drawback of using different imaging systems.
2005	Moon et al.	Anisotropic diffusion filtering and stick method Thresholding - level set method Feature extraction - contour difference, shift distance, area difference and solidity Classification - support vector machines	Continuous and non-continuous images were compared for tumor classification.
2005	Song et al.	Feature extraction - margin sharpness, margin echogenicity, angular continuity, tissue attenuation, mass attenuation, and excess attenuation Classification - artificial neural networks, logistic regression	Logistic Regression is superior in high sensitivity region and neural networks work better in high specificity region.

Chapter 3

MULTI-OBJECTIVE OPTIMIZATION BASED IMAGE THRESHOLDING

Image segmentation is an important step in image analysis since the result of segmentation plays a vital role in feature extraction. Image segmentation is defined as the process of extracting information from an image by partitioning the image into multiple regions. Segmentation is performed based on grey level intensities of the image. Image thresholding is an easy and simple image segmentation technique. This method partitions an image into regions based on a predefined criterion. The challenging aspect of image thresholding is to select a suitable threshold. Many strategies are available to select the threshold. One common strategy is to make use of the image histogram to choose the threshold. An image histogram is based on the number of pixels that have the same grey level intensity value. Single objective optimization (SOO) has been used to find a suitable threshold based on the image histogram. There are different methods that use SOO to find a suitable threshold. Some available methods are Otsu method, minimum error method, mode method and entropy method. In this method, Otsu method and minimum error method are used because their performance is better than entropy and mode method in most cases. Two methods used in this work are explained in detail.

3.1 Optimization based on single objective

3.1.1 Otsu method

Otsu developed a method for obtaining an optimal threshold based on maximizing the inter-class variance (Otsu 1979). This method involves calculating the variance of the two classes of pixels at all possible threshold values. The objective of the method is to maximally separate the two types of pixels. The optimum threshold is obtained by maximizing the between class variance.

For a given image, an image histogram is calculated such that the number of pixels at each grey level i is denoted by n_i. N is the total number of pixels in the image and L is the number of grey levels in the image. The histogram is normalized into a probability distribution.

$$p_i = n_i/N \tag{3.1}$$

The zeroth and first-order cumulative moments of the histogram up to the k^{th} grey level are given by equations 3.2 and 3.3, respectively, and the total mean level of the original image is given by equation 3.4.

$$\omega(k) = \sum_{i=1}^{k} p_i \tag{3.2}$$

$$\mu(k) = \sum_{i=2}^{k} ip_i \tag{3.3}$$

$$\mu_T = \mu(L) = \sum_{i=1}^{L} ip_i \tag{3.4}$$

The objective function for maximizing the between class variance is

$$\sigma_B^2(k) = \frac{[\mu_T\omega(k) - \mu(k)]^2}{\omega(k)[1 - \omega(k)]} \tag{3.5}$$

The k value for which equation 3.5 is maximized is the optimum threshold T, where $1 < k < L$.

3.1.2 Minimum error method

In this method, a classification approach is used to select a suitable threshold. If the grey level distribution of the object and background can be estimated, the minimum error based threshold can be obtained. The assumption used in this method is that the estimated object and background populations are normally distributed. Based on this assumption, Gaussian curves can be fitted for the object and background distributions by estimating their mean, standard deviation and probability and thereby obtaining the optimum threshold.

Kittler and Illingworth (Kittler & Illingworth 1986) proposed a simple technique using the above concept. In this method, the image is represented by a histogram denoted by $h(g)$. Here, thresholding is performed on the image at some arbitrary level T; then the resulting object and background populations can be modeled by a normal distribution $h(g)$ with parameters $\mu_i(T)$ and $\sigma_i(T)$ and *a priori* probability $P_i(T)$. The parameters are defined by equations 3.6, 3.7 and 3.8.

$$P_i(T) = \sum_{g=a}^{b} h(g) \tag{3.6}$$

$$\mu_i\left(T\right) = \left[\sum_{g=a}^{b} h\left(g\right) g\right] / P_i\left(T\right) \tag{3.7}$$

$$\sigma_i^2(T) = \left[\sum_{g=a}^{b} \{g - \mu(T)\}^2 h(g) g\right] / P_i(T) \tag{3.8}$$

where a and b are given by equations 3.9 and 3.10, respectively

$$a = \begin{cases} 0 & i = 1 \\ T+1 & i = 2 \end{cases} \tag{3.9}$$

$$b = \begin{cases} T & i = 1 \\ n & i = 2 \end{cases} \tag{3.10}$$

The function to be minimized for obtaining the optimal threshold is given by equation 3.11. The equation represents the probability of error between the actual histogram and the assumed object and background distributions.

$$J(T) = 1+2[P_1(T)\log\sigma_1(T)+P_2(T)\log\sigma_2(T)]-2[P_1(T)\log P_1(T)+P_2(T)\log P_2(T)] \tag{3.11}$$

The optimal threshold is found by selecting T such that the above function returns a minimum value.

3.2 Multi-objective optimization

The segmentation process is often always based on the optimization of a single objective function (Sahoo et al. 1988). The segmentation performed based on the above mentioned methods works well for many cases. However, each method has its own limitations. Otsu method breaks down when the sizes of the two classes are very unequal resulting in more than one maxima and consequently missing the global threshold (Bebis 2004*c*). Kittler method fails when the two histogram modes are not distinguishable as the result of bias due to the estimation of mean and variances from the truncated distribution (Sezgin & Sankur 2004). The weakness of the individual methods can be improved by applying a hybrid approach involving both the objectives to improve the segmentation process. Hence, a multi-objective optimization problem can be solved to obtain an optimum threshold.

Multi-objective optimization (MOO) is the process of optimizing two or more conflicting objectives simultaneously subject to certain constraints. MOO has applications in various fields such as product design, medical, automobile, oil and gas

industry, etc (Rangaiah 2009). MOO is performed where decisions are to be taken by a trade-off between the conflicting objectives. Upon solving a MOO problem, a set of solutions known as the Pareto front is obtained. Based on the knowledge of the system and the user requirement, the user can select a solution from the Pareto front for implementation. A Pareto front is defined as a set of solutions which are non-dominated to each other, i.e. any solution in the set cannot replace another solution in the set to improve an objective without worsening another objective. For example, let us consider a MOO problem with two conflicting objectives f_1 and f_2 that are to be minimized. Upon solving the problem, we can obtain a solution vector $x = [x_1, x_2, x_3, x_n]$. A solution x_i is said to be dominating another solution x_j, if the conditions $f_1(x_i) < f_1(x_j)$ and $f_2(x_i) < f_2(x_j)$ hold true. A solution x_i is said to be a Pareto solution, if there doesnt exist any solution x_j such that it dominates x_i within the solution space (Tamaki et al. 1996, Miettinen 1999).

There are many methods available to solve MOO problem. Some methods used for obtaining Pareto optimal solutions are weighting method, ϵ-constraint method, non-dominated sorting genetic programming (NSGA-II), etc. The first two approaches convert the MOO problem into a SOO problem and solve the problem using SOO problem solving methods (Miettinen & Hakanen 2009). NSGA-II is an evolutionary algorithm, inspired by the natural evolution process (Srinivas & Deb 1994). In this method, a population of solutions is generated stochastically and then this population is evolved through genetic operations into a more appropriate solution over several generations.

3.2.1 Converting a MOO problem into a SOO problem

In this method, the weighted sum approach is used to solve the MOO problem. The weighted sum method is the simplest method to solve a MOO. This method can be used to solve a MOO when the problem solution is convex (Miettinen & Hakanen 2009). In this approach, the set of objectives is scalarized into a single objective

by multiplying each objective with the help of a certain weight and aggregating the objectives together. The formulation of the weighted sum approach is given by

$$\begin{aligned} &minimize \sum_{i=1}^{k} w_i f_i(x) \\ &subject\ to\ x \in S \end{aligned} \tag{3.12}$$

The conditions to be considered for applying this method.

1. Objectives are normalized in order to scale them to the same magnitude.
2. Weights must be nonnegative and must lie between 0 to 1, that is, $w_i \in [0, 1]$.
3. Sum of all weights should be equal to 1, that is $\sum_{i=1}^{k} w_i = 1$.
4. For mixed optimization problems (min-max), we need to convert all the objectives into a single type.

A Pareto front can be obtained by solving the SOO for different values of the weights. The weights are also known as importance factors as they measure the importance of each objective in the process. The problem is solved for many discrete values of weights in the range [0, 1]. The solution obtained is considered Pareto optimal if the weighting coefficients are positive. Based on the users requirement, he/she can select a solution from the Pareto front. In our work, we have used simulated annealing to solve the SOO problem obtained by converting the MOO problem.

3.2.2 Simulated annealing

Simulated Annealing (SA) is a random search method used for obtaining global optimum in a search space and is employed mainly for handling discrete optimization problems (Dowsland 1993). This method was inspired from the idea first presented by Metropolis et al. (Metropolis et al. 1953) in 1953 to simulate the metal annealing process. Annealing is a heat treatment technique to cause changes in the structural

properties of a solid. This process is carried out by heating the material above its melting point and sustaining a suitable temperature and then cooled back to the solid form. The slow cooling allows the process to reduce the defects in the material. On rising the temperature, the atoms are freed from their initial locations and randomly move through states of higher energy; the slow cooling process allows the atoms to find a lower energy state than the initial states. Such a process is simulated by considering the material as a system of particles. Metropolis et al. simulated the change in energy of the system while the system is cooled till it reaches a steady state. Metropolis et al. calculated the new energy state and then compared it to the current state. If the energy has decreased, it is accepted as the next state. If the energy has increased, then the new state is accepted as the next state according to a probability function. This probability is defined based on the law of thermodynamics. At any temperature t, the probability of an increase in energy by magnitude δE is given as

$$p(\delta E) = \exp\left(-\frac{\delta E}{kt}\right) \tag{3.13}$$

where k is the Boltzmann constant. The process of calculating the new state is repeated for a number of iterations at each temperature after reducing the temperature at a given rate till the system reaches a steady state. Kirkpatrick et al. (Kirkpatrick et al. 1983) and Černý (Černý 1985) independently applied this strategy to search for global optimum in optimization problems by comparing the problem with the cooling process.

Local search algorithms like hill descent method end up obtaining local optimum for the optimization problem based on the initial guess solution. To overcome this limitation, a few uphill moves can be performed based on a probability criterion to move towards the global optimum. The difference between the random descent method and simulated annealing method is that the annealing method allows a few uphill moves based on the probability calculated by equation 3.13.

The algorithm for simulated annealing can be summarized as:

1. Select an initial state s_0. Calculate the energy of the state $f(s_0)$.

2. Select an initial temperature $t_0 > 0$.

3. Select a rate of cooling α.

4. Randomly select a new state s from the neighborhood of s_0. Calculate the energy of the new state, $f(s)$.

5. If $f(s) < f(s_0)$ then take $s_0 = s$. Else generate random number g uniformly distributed in the range [0, 1]. Check if $g < \exp((f(s0) - f(s))/t)$, then take $s_0 = s$. Otherwise stay at state s_0. Repeat the steps 4 and 5 until a certain number of iterations are performed.

6. Reduce the temperature at a certain cooling rate and repeat steps 4 to 6 till a steady state temperature is reached; s_0 is the approximation to the optimal solution.

The flow sheet of this algorithm is shown in the Fig. 3.1.

3.3 Problem formulation

The objective of the optimization process here is to find the optimum threshold value that can be used to best segment the grey level image. Two objectives are considered here. One of the objectives is to maximize the inter-class variance and the other objective is to minimize the error. This is a mixed optimization problem. Therefore, the first objective is changed appropriately into a minimization problem - the final objective required to be minimized is therefore formulated as in equation 3.14.

$$F(t) = w_1 * \frac{1}{{\sigma^2}_B(t)} + (1 - w_1) * J(t) \tag{3.14}$$

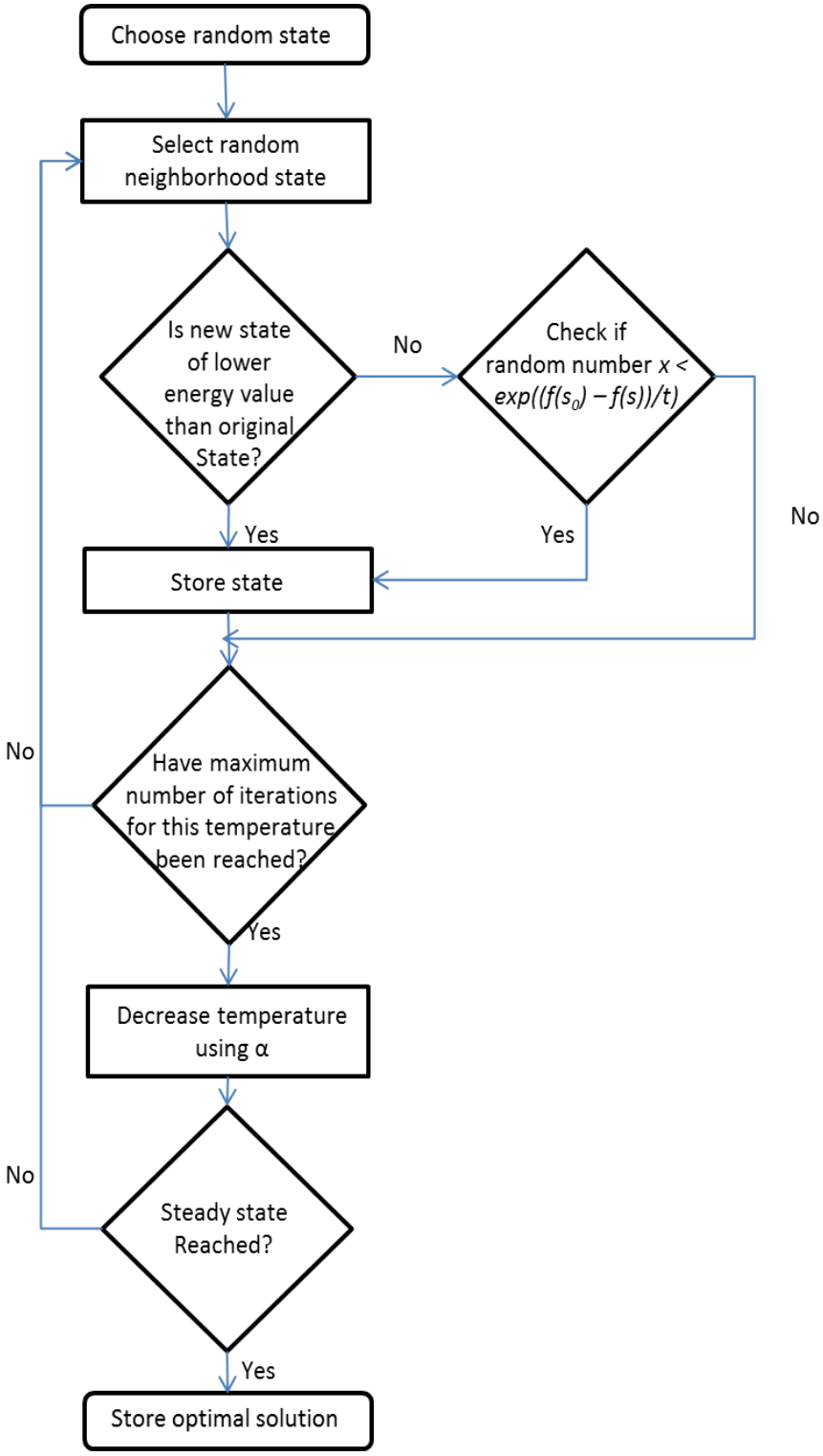

Fig. 3.1. Steps involved in simulated annealing

where σ_B and J are defined as in equations 3.5 and 3.11 respectively.

Both the objective functions are normalized to similar magnitude in order to avoid biasing the main function. The search space varies from 0 to 255 indicating the grey level intensities of the image. Though the problem is of the type of combinatorial optimization, exhaustive enumeration cannot always be used to search the entire solution space due to high computational cost. Therefore, simulated annealing is used to determine the global optimum. Due to the annealing process, this method can find the global (or near global) optimum for problems which have numerous local optima. The optimization is carried out by varying the weight w_1 from 0 to 1. Since the Pareto optimal front for this problem is convex, the weighted sum method gives the Pareto frontier.

Once a Pareto front is obtained, an optimal solution can be selected based on *a priori* knowledge. Since we do not have any *a priori* knowledge to select an optimal solution, post-Pareto-optimality analysis is carried out using the L_2-norm method to find an optimal compromise solution (Kasprzak & Lewis 2001). This method uses the concept of utopia point to find the optimal solution. Utopia point is defined as the theoretically best achievable point and is assumed to be the origin in most cases. In our approach, L_2-norm method finds the solution that is geometrically closest to the utopia point (assumed to be the origin).

The segmentation quality is evaluated by calculating the error in pixel classification. The error in pixel classification is found by calculating the sum of number of pixels wrongly classified (i.e. background pixel classified as object and object pixel classified as background) (Bhanu et al. 1995). In this thesis, all the image analysis steps were performed in Matlab 7.11.0 (R2010b).

3.4 Results and discussions

In this work, the above explained MOO based segmentation along with morphological operations was tested on several images. Two examples are shown and the results are discussed. The pre-processed images were segmented by three different

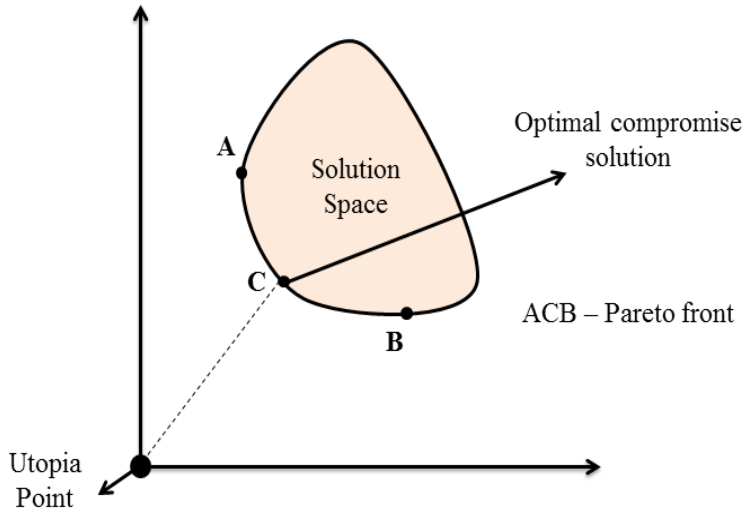

Fig. 3.2. Illustration of the L_2-norm based optimal compromise solution extraction from the Pareto front

methods: (i) Otsu method, (ii) minimum error method, and (iii) Multi-objective optimization based segmentation method and the results are compared with each other.

3.4.1 Example 1

A greyscale image of a spider is taken to test the algorithm. The image is shown in Fig. 3.3[1]. The MOO problem is solved for different values of weight w_1.

The Pareto front is obtained by plotting the first objective function along the x-axis (in logarithmic scale) versus the second objective function along the y-axis. The optimal threshold obtained using the L_2-norm method is shown in the Pareto plot given in Fig. 3.4. The thresholded image obtained from Otsu and minimum error method is shown in Fig. 3.5(a) and (b), respectively.

The image obtained by thresholding using the optimal threshold calculated by the MOO method is given in Fig. 3.5(c). From Fig. 3.5(a), it is clear that Otsu

[1]Image Courtesy: Wikimedia Commons

Fig. 3.3. Image - Example 1

method segments the complete region of interest, but fails to differentiate between the darker pixels of the background and the image of the spider. Similarly, from Fig. 3.5(b), it can be said that the shape of the spider is identified. In Fig. 3.5(c), it can be seen that MOO based thresholding not only identifies the complete outline of the spider but also identifies some pixels which are missed out by the minimum error method. This comparison can be further verified by calculating the misclassification rate of each segmentation method. The misclassification rates of the three thresholding methods for this example is shown in the first row of Table 3.1. From Table 3.1, it is clear that thresholding based on MOO is better than thresholding based on Otsu method by a significant extent. The MOO based method outperforms the minimum error method albeit by a small amount.

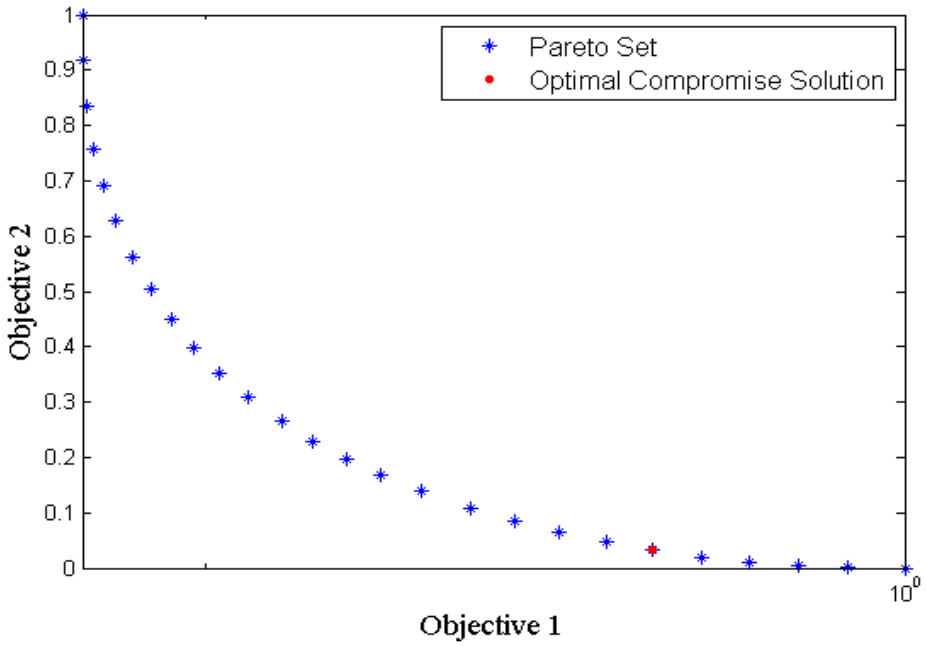

Fig. 3.4. Pareto plot - Example 1

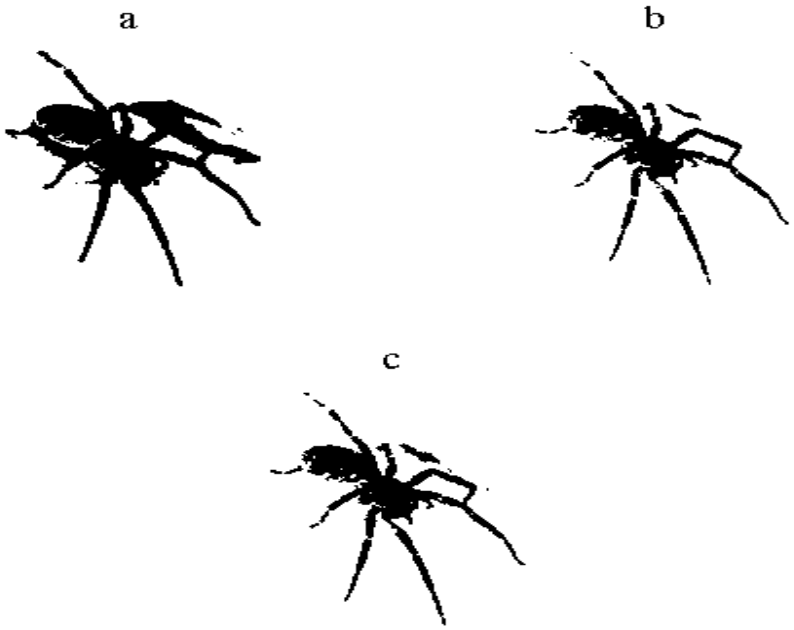

Fig. 3.5. Example 1: (a) - Otsu method (b) - Minimum error method and (c) - MOO based segmentation

3.4.2 Example 2

An infrared image of an aircraft model shown in Fig. 3.6[2] is taken for segmentation.

Fig. 3.6. Image - Example 2

The Pareto front (shown in Fig. 3.7) is obtained by plotting the objective function values in a fashion similar to example 1. Optimal threshold obtained using the L_2-norm method is used for the segmentation of the actual image. In the Pareto plot, it can be noted that there is a gap between the set of Pareto solutions. This shows that those regions do not contain non-dominated solutions. The thresholded images obtained from the three methods are shown in Fig. 3.8(a), (b) and (c) respectively. In this example, it is clear that Otsu method captures the outline of the aircraft while the minimum error method based thresholding captures the shape of the aircraft precisely along with some noise in the background. From Fig. 3.8(c), it can

[2]Image Courtesy: ThermoAnalytics.com - reproduced with permission

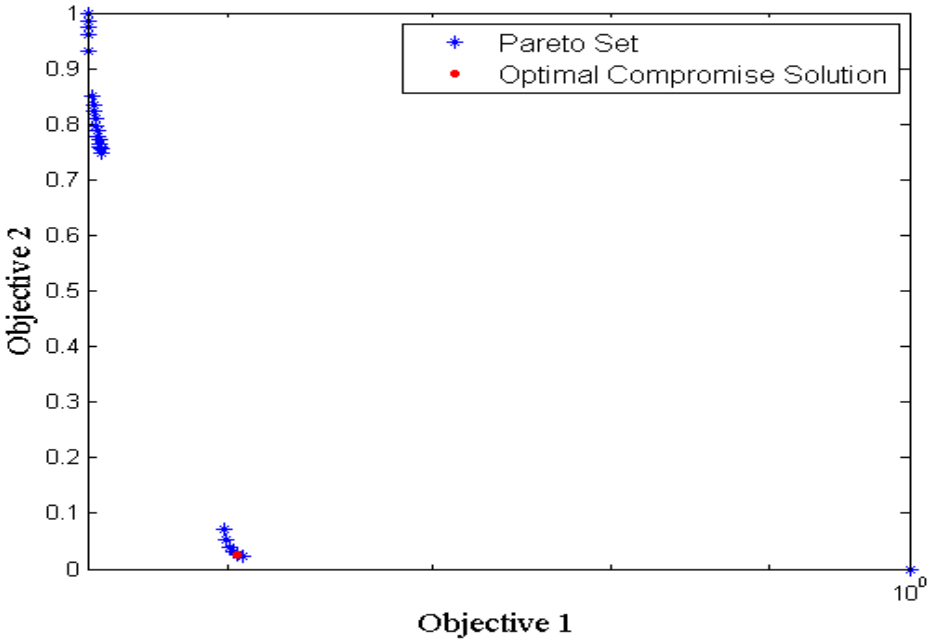

Fig. 3.7. Pareto plot - Example 2

be seen that MOO based thresholding captures the shape of the aircraft completely and avoiding the noise captured by minimum error method. The performance is validated from the misclassification rates shown in the last row of Table 3.1.

In Table 3.1, it can be noticed that misclassification rate of minimum error method is higher compared to the Otsu method and MOO based thresholding method. The misclassification rate confirms the fact from the figures that Otsu method outperforms the minimum error method, while MOO based thresholding fares better than both the methods.

Table 3.1
Misclassification rate for general images

Image Name	Otsu Method	Minimum Error Method	MOO based segmentation
Example 1	56.34	18.83	16.67
Example 2	19.29	59.63	1.49

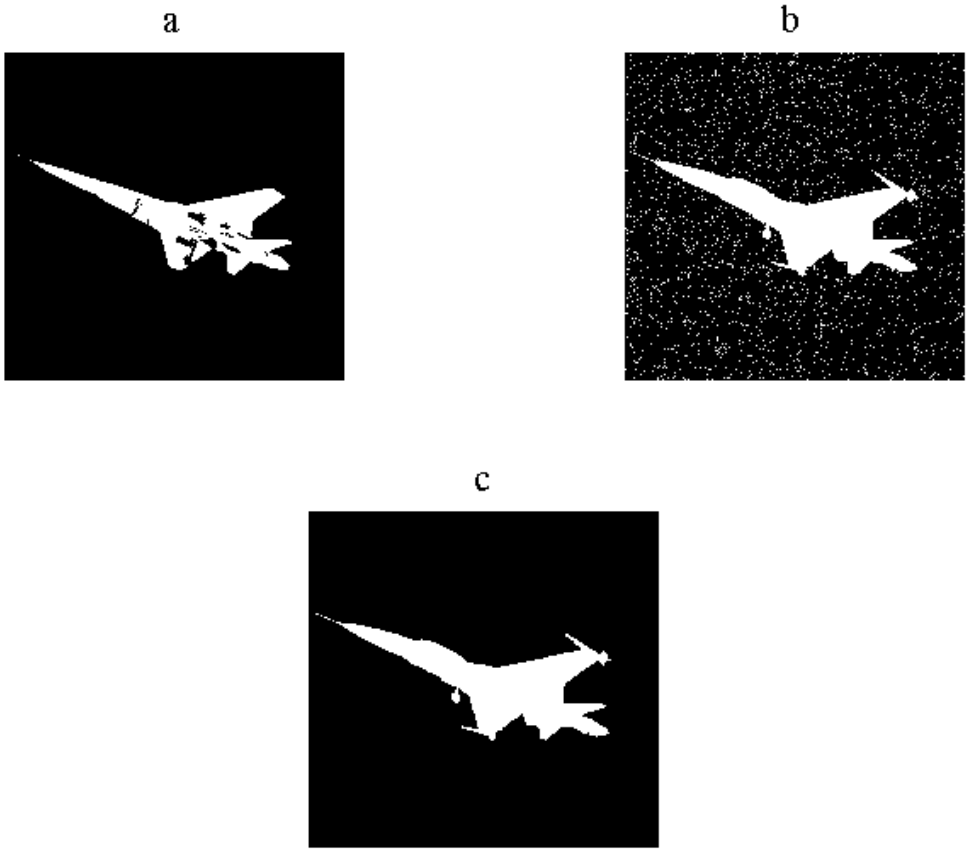

Fig. 3.8. Example 2: (a) - Otsu method (b) - Minimum error method and (c) - MOO based segmentation

From Fig. 3.5, 3.8 and Table 3.1, it can be said that Otsu method performs better than the minimum error method when the object is lighter than the background and vice versa. The MOO based thresholding approach is found to be very effective for thresholding different types of images. This method was tested on several other examples and case studies to check the effectiveness of the algorithm. Therefore, the proposed method may be very useful for solving real world image analysis problems.

Chapter 4

IMAGE ANALYSIS APPLICATIONS FOR REAL-WORLD PROBLEMS

Image analysis plays a major role in various fields like manufacturing and medical imaging. Machine vision is regarded as one of the strategic technologies in manufacturing industries due to increasing demands to maintain high quality of the product (Steger et al. 2008). Machine vision applications include quality and process control in manufacturing process. In a crystallization process, process control plays a vital role to obtain crystals of desired quality - size, shape, morphology etc. CSD is one of the characteristics to be monitored at continuous intervals for crystallization process control. Image analysis methodologies can be used to estimate CSD from PVM images and contribute to improved control of an ongoing crystallization process. In this chapter, we will show how the MOO based segmentation method can be applied to perform inline monitoring, based on images obtained from a simulated crystallization process.

Medical image analysis is used to extract meaningful information about the physiological processes or organs of the body (Dhawan 2011) by analyzing the images obtained using medical imaging. Medical imaging is the process of acquiring images of the body using different imaging techniques such as ultrasound, radiology, magnetic resonance imaging (MRI), etc. The purpose of medical image analysis is either for diagnosing the body for illness or to develop medical science (to study the normal functioning of the body). The main advantage of medical imaging is that it is considered as a non-invasive procedure to investigate the internal parts of the body to design and develop methodologies for the diagnosis of diseases.

In this chapter, image analysis is applied to two case studies. The first case study involves the estimation of crystal size distribution (CSD) from PVM images. In this work, artificial images representing crystals from a crystallization process are generated. Then, CSD is estimated using MOO based image thresholding followed by feature extraction. The obtained CSD from the automated procedure is compared with the actual CSD used to generate the artificial images. The second application concerns the automated classification of breast tumors using ultrasound images. MOO based thresholding approach is applied to the breast ultrasound images followed by feature extraction to obtain the properties (such as size, shape, etc.) of the tumor. These properties can assist radiologists while classifiying the breast tumor (as benign or malignant). MOO based thresholding approach has not been used for segmentation previously for such problems. Therefore, this thesis applies such MOO based approach to improve the segmentation quality for achieving better detection and diagnosis of tumors.

4.1 Case I - Estimation of crystal size distribution: image thresholding based on multi-objective optimization

The motivation for this problem has been discussed in detail in Section 2.5. Here, application of image analysis on the crystallization process images is described along with its results. The objective is to estimate the CSD from the simulated images and validate the algorithm with data used to generate artificial images.

4.1.1 Image acquisition

Artificial images were generated randomly by considering a certain camera model to depict the assumed process model.

Camera model

The method of mapping points from a real world 3-dimensional plane onto an imaginary 2-dimensional plane is known as projection. When the human eyes look at a scene, objects farther away appear smaller than the objects close by-this property is known as perspective. Orthographic projection is a projection method where the object is mapped onto an imaginary plane without considering the distance of the object from the observer. Orthographic projection is used to create images to scale drawings. This projection allows making accurate measurements. When a perspective projection is approximated using a scaled orthographic projection, it is known as weak perspective projection. This projection is considered when the objects dimensions are small compared to its distance from the camera. The camera model is explained in the literature (Bebis 2004*a*).

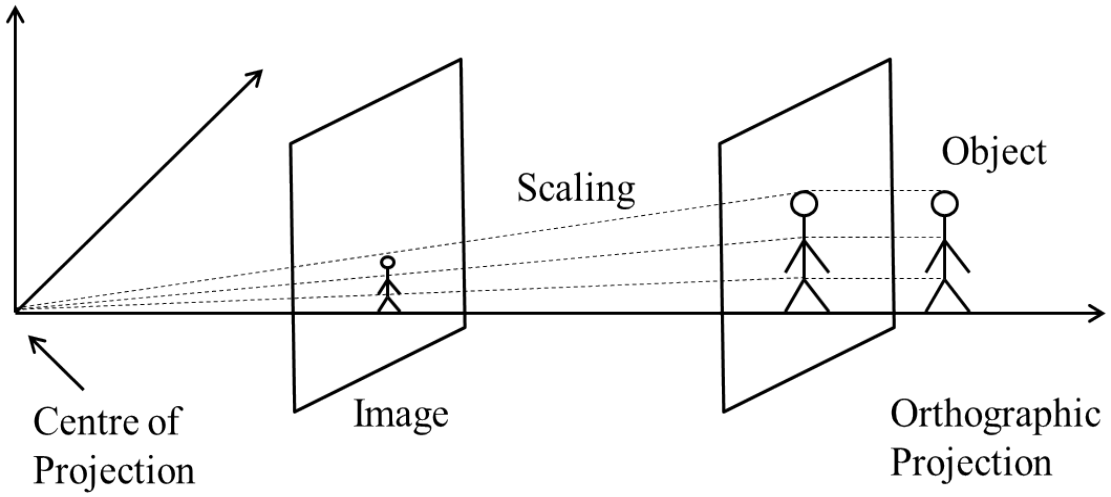

Fig. 4.1. Weak perspective projection

Process model

The first step is to define a process model bearing in mind certain number of assumptions. In this work, the particles are assumed to be needle shaped. Generally, needle shaped crystals are observed in crystallization processes involving monosodium glutamate, calcium pyrophosphate dehydrate, monosodium urate, etc. Solid phase particles dispersed in a crystallization solution bath is assumed to be the process model. Let us assume a volume V to be the imaging volume captured by the camera. Assume n solid particles are captured in the imaging volume. Let the characteristic length of each particle in the given volume be denoted by l. Hence, the CSD in the imaging volume is given by a function $f(l)$.

In this process model, the particle population is simulated by randomly generating several parameters such as the position of the particle, orientation of the particle and dimensions of the particle. The orientation of the particle in the image plane is distributed normally. The dimensions and position of the particle in the image plane are distributed uniformly for illustrative purposes. The parameters are generated randomly independent of each other.

The transformation from a 3D point X, Y and Z in real-world coordinates to an image point x_I and y_I is given by equation 4.1, where f_l is the focal length of the camera.

$$x_I = \frac{f_l X}{Z}; y_I = \frac{f_l Y}{Z} \tag{4.1}$$

Assumptions

The real world coordinates are mapped into coordinates on the image plane. It is assumed that the depth of the imaging volume is very small compared to the fixed distance between the camera and the imaging volume since the distance of the camera from the particle will be greater than the depth of the particle. Hence, weak

perspective projection model is used to project the imaging volume onto the image plane. The particles are scaled by a constant ratio.

Generally, the crystallization process is assumed to take place in a well stirred vessel, and hence the particles are expected to align parallel to the surface of the solution due to the shear force between the surface of the particle and the solution. Therefore, the particles are assumed to be orthogonal to the cameras optical axis and thereby mimic the actual condition used for imaging measurements. A similar artificial image generation technique was used in (Larsen & Rawlings 2008) to simulate crystallization images. However, in contrast to the work presented in (Larsen & Rawlings 2008), in our work, the intensity values of the background and particles are also generated stochastically. Also, more importantly, in our work, noise is incorporated in to the generated images so as to mimic images obtained from industrial crystallization processes.

The intensities of the slurry and the particles were generated randomly independent of each other and distributed uniformly. Particle overlaps were also added to the system stochastically. Speckle noise (process noise) of mean = 0 and variance = 0.02 was added into the image plane. Some broken particles and small particle chips were also added randomly to the image plane. Imaging volume is taken to be large enough so that all the particles generated stochastically are contained within the imaging plane itself. Hence, limits have been set while generating the coordinates and dimension of the particle so as to make sure the generated particle remains within the imaging plane. An image generated with the help of the above algorithm along with an image from a real crystallization process is shown in Fig. 4.2.

4.1.2 Image pre-processing

Generally, a digital image is represented as a three dimensional matrix indicating each of the basic colors red, green and blue. These images are first converted to single dimensional matrix for further processing. The single dimensional matrix represents

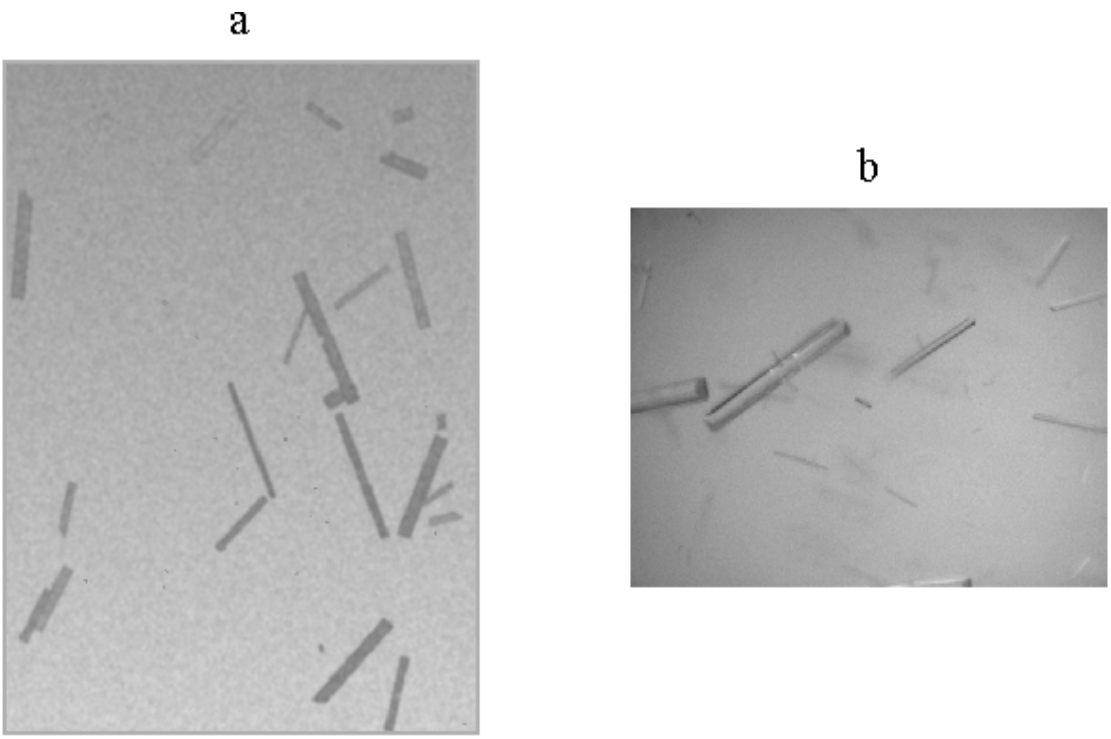

Fig. 4.2. (a) Artificial image (b) Real-world image

the grey level intensity at each pixel. The grey level matrix GL is computed as the weighted sum of the three dimensions (red R, green G and blue B) given by equation 4.2 (Nagabhushana 2006).

$$GL = 0.299 * R + 0.5870 * G + 0.1140 * B \tag{4.2}$$

The objectives of pre-processing include noise removal and image enhancement. The grayscale images contain a considerable amount of noise. Generally, image noises in crystal images are due to the sensitivity of camera and during data transfer and storage (file formats). The types of noise associated with this type of images cannot be removed with the help of a linear filter. Therefore, a type of non-linear filter called the median filter is used to remove noise from the images considered in this work. This type of filter is useful in removing impulse and speckle noise

(Gonzalez & Woods 2008). This type of filter has the additional advantage of preserving the edges of objects and is very apt for the current application.

The other purpose of pre-processing is to enhance the quality of the image. Contrast enhancement is applied to images to widen the range of the grey level intensity.

4.1.3 Image segmentation

In this work, image segmentation is performed based on the method explained in Chapter 3. Morphological operations are performed on the binary image to remove unwanted disturbances such as broken particles and small chips. This methodology was tested on several images. Two examples are shown and the results are discussed. The pre-processed images were segmented by three different methods (i) Otsu method, (ii) minimum error method, and (iii) Multi-objective optimization based segmentation method and the results are compared with each other. In this work, the original Otsu and minimum error methods are used without any modifications (Otsu 1979, Kittler & Illingworth 1986).

Example 1

In the first example, we consider an image with few crystals, considering that the process is in the initial stages. The MOO problem is solved for different values of weight w_1.

The Pareto front is obtained by plotting the first objective function along the x-axis on logarithmic scale versus the second objective function along the y-axis. From Fig. 4.3, it can be observed that there is a gap in the Pareto front, which shows that there is no non-dominated solution in that space. The optimal threshold is obtained by using the L_2-norm method. This threshold is used for the segmentation of the process image shown in Fig. 4.4(a). The image obtained after thresholding using the Otsu and minimum error methods are shown in Fig. 4.4(b) and (c), respectively.

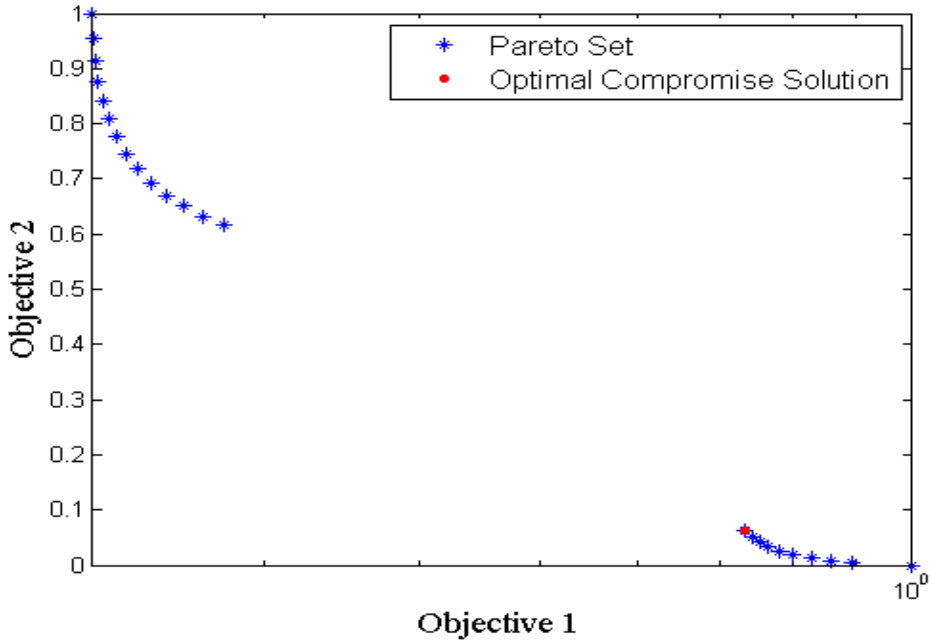

Fig. 4.3. Pareto plot - Crystallization example 1

The image obtained by thresholding using the optimal threshold calculated by the MOO method is given in Fig. 4.4(d). From Fig. 4.4(d), it is clear that Otsu method segments the particles of darker intensity clearly, but while dealing with lighter intensity particles it fails to differentiate between the background and the object. Similarly, from Fig. 4.4(c), it can be said that outline of the most particles are identified but the complete shape of the particles are not characterized properly. In Fig. 4.4(d), it can be seen that MOO based thresholding overcomes the limitations of the other methods and identifies most particles completely. This comparison can be further verified by calculating the misclassification rate of the segmentation method. The misclassification rates of the three thresholding methods are shown in Table 4.1. From row 1 of Table 4.1, it is clear that the misclassification with the MOO approach is very less compared to the misclassification when the thresholding is based on Otsu or minimum error method.

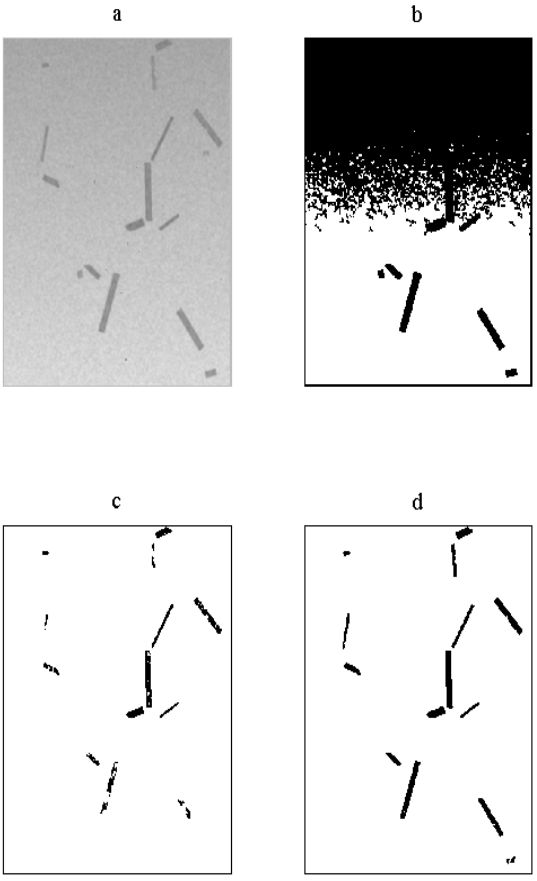

Fig. 4.4. Crystallization example 1 (a) - Original image, (b), (c), (d) Image after thresholding using Otsu method, Minimum error method, and MOO based segmentation respectively

Example 2

In the second example, the number of particles in the image is increased. This is to simulate the later stage of a crystallization run during which we expect to have more crystals in the crystallizer.

The Pareto front (shown in Fig. 4.5) is obtained similar to example 1. Optimal threshold obtained using the L_2-norm method is used for the segmentation of the process image shown in Fig. 4.6(a). The images obtained after thresholding using the three considered methods (Otsu, minimum error and MOO based approach) are shown in Fig. 4.6(b), (c) and (d) respectively. Similar to what was seen in example

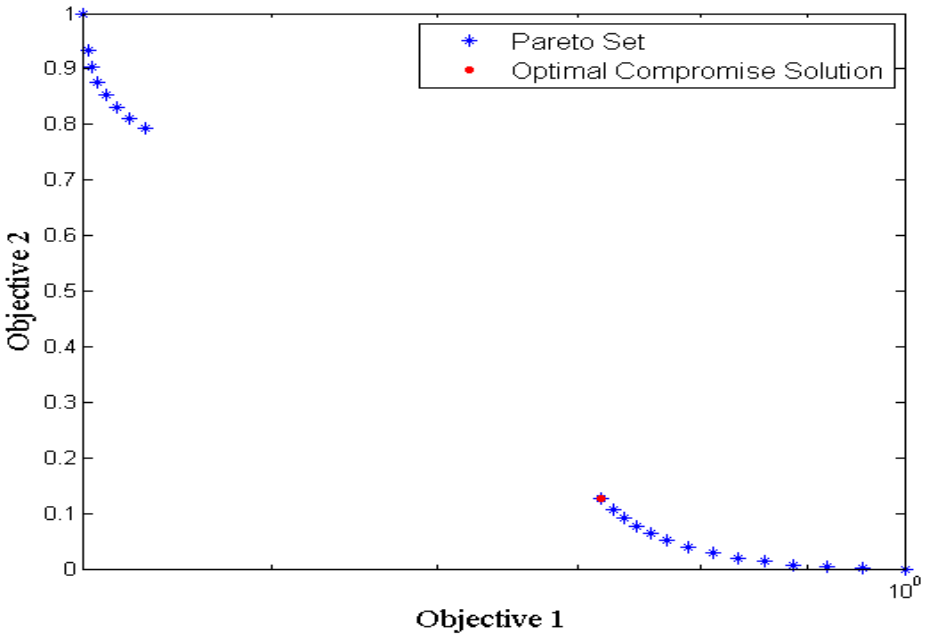

Fig. 4.5. Pareto plot - Crystallization example 2

1, it is clear that Otsu method based thresholding fails to differentiate between the particle and the background while minimum error based thresholding doesnt capture the particle contour as well as one would have hoped for. From Fig. 4.6(d), it can be seen that MOO based thresholding performs better than the other two methods. The performance is validated using the misclassification rates as indicated in the last row of Table 4.1.

From the results shown in Table 4.1, it can be noticed that misclassification rate of Otsu method is much higher compared to the minimum error method and MOO based thresholding method. The misclassification rates confirm that minimum error method performs better than Otsu method, while MOO based thresholding outperforms both the methods. From Table 4.1, it can also be noted that, as expected, the misclassification rate increases as the number of particles in the image increases.

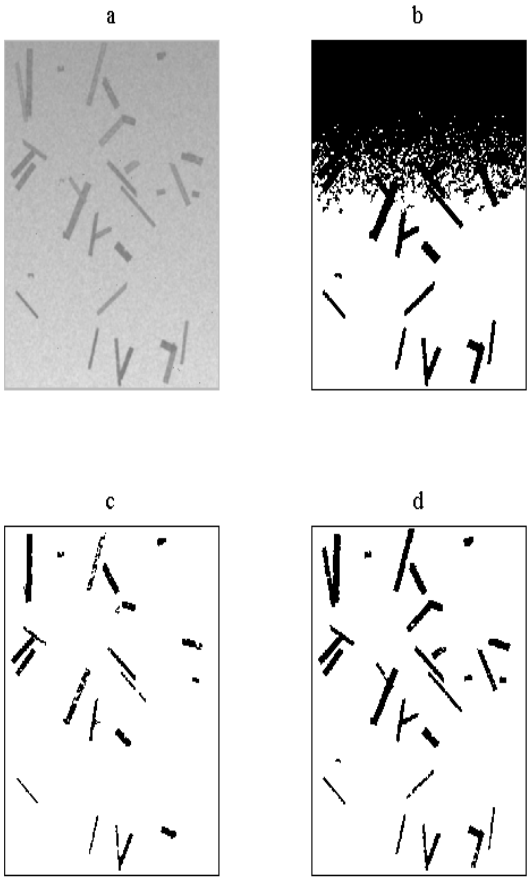

Fig. 4.6. Crystallization example 2 (a) - Original image, (b), (c), (d) Image after thresholding using Otsu method, Minimum error method, and MOO based segmentation respectively

Table 4.1
Misclassification rate for crystallization images

Image Name	Otsu Method	Minimum Error Method	MOO based segmentation
Example 1	48.38	1.73	0.4
Example 2	37.15	5.58	1.34

4.1.4 Feature extraction

The characteristic length of each segmented object has to be calculated. Hence, the feature extraction step is used to extract features of the segmented objects. Blob

Analysis is used for feature extraction (Instruments 2008). In the binary images, the objects are denoted by 1 and the background is denoted by 0. The pixels which have same values that are connected (touching particles) are referred to as blob. Separate objects are referred to as different blobs in the image. Using blob analysis, one can find numerous statistics such as the number of blobs, position of the blobs, area of each blob, etc.

In blob analysis, the minimum area rectangle algorithm is used such that the bounding box encloses the polygon (shown in Fig. 4.7). The features of this bounding box are taken as the properties of the blob. The minimum area rectangle is found using the rotating calipers method (Toussaint 1983) as described in algorithmic form below.

The algorithm for minimum area rectangle is explained briefly.

1. Find four extreme points for the polygon.

2. Draw lines of support through each of these four points parallel to the x and y axes so as to form a rectangle enclosing the polygon. These lines make a certain angle with different edges of the polygon.

3. Rotate the lines in clockwise direction so that one of the lines coincides with an edge of the polygon.

4. Compute the area of the new rectangle and compare it to the minimum area. If the current area is smaller than the minimum, store this as the new minimum.

5. Repeat steps 3 - 4 until the total rotation of the lines is greater than 90 degrees.

6. From this method, the required minimum area rectangle enclosing the polygon is obtained.

With the help of blob analysis, the CSD was estimated from the process images. This method was tested on numerous images and is illustrated using the image used as Example 2 above. The example image is given in Fig. 4.8(a). The image after

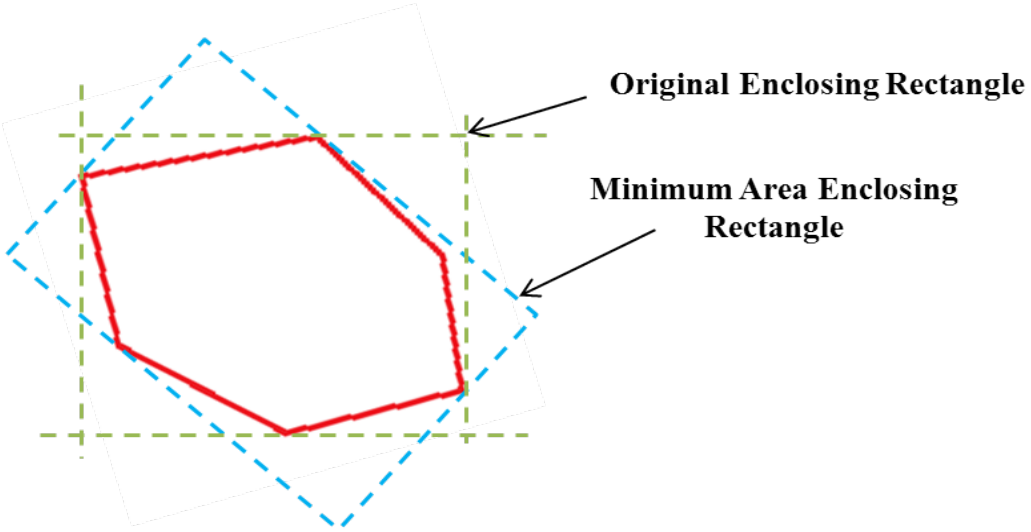

Fig. 4.7. Minimum area enclosing rectangle

segmenting using the MOO approach undergoes morphological processing and is given in Fig. 4.8(b). The final image where the individual particles are identified is given in Fig. 4.8(c).

The accuracy of the proposed method was found by comparing the estimated CSD with the true (known) particle characteristics (true CSD) used to generate the artificial images. The estimation accuracy in an image is calculated by computing the sum of absolute error between the actual length and the characteristic length of each particle estimated by the algorithm. The estimation accuracy was tested on different sets of images by varying the number of particles in the process images. The algorithm was tested for 3 different sets of 100 images representing different size ranges. The results are compiled in Table 4.2. The last three columns presented in Table 4.2 gives the mean, maximum and minimum estimation accuracy with respect to the number of particles that exist in each image (given in first column). As the number of particles increased, it was noted that there is an increase in the percentage of overlapping particles in the image. Hence, the percentage overlap was calculated for each set of images as the ratio of number of particles that are overlapped in the image to the actual number of particles and the average percentage overlap is

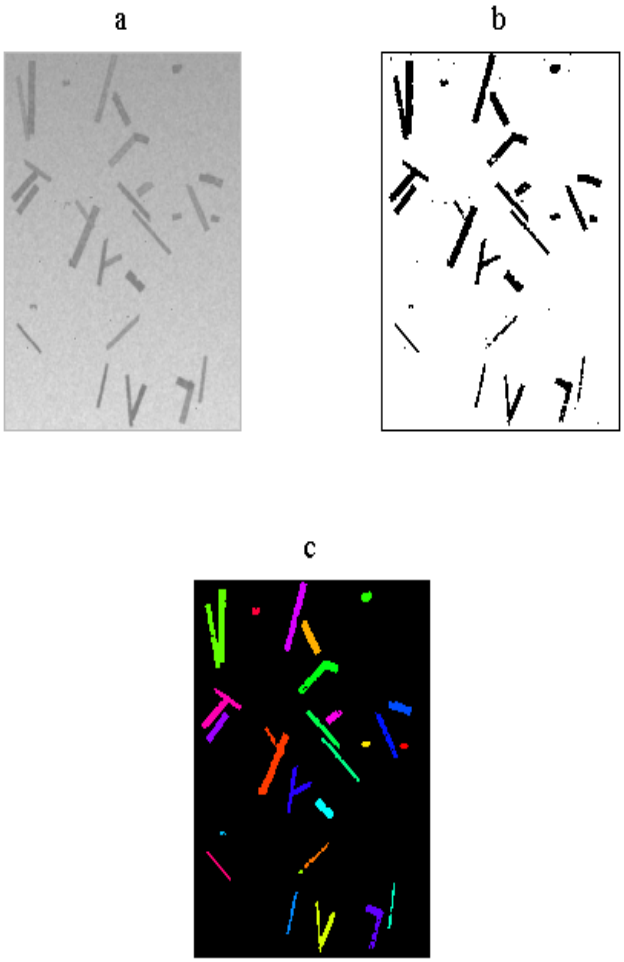

Fig. 4.8. (a) Original image, (b) Segmented image, and (c) Final image

presented in the second column in Table 4.2. The mean accuracy of the proposed MOO-based algorithm was found to be higher than 95% when 5-15 particles exist in an image. The mean accuracy dropped down to around 92.7% when the number of particles in the image increased to 20-25 particles. Hence, it can be seen that the particle size characteristics are captured very well by this method in each image. In this work, the overlapped particles have been not been taken into consideration for calculating the estimation accuracy.

In PVM, a set of images are captured by the camera at successive time points till we have enough information to estimate the CSD which is very crucial for effective

Table 4.2
Estimation accuracy for different sets of crystallization images

No. of particles	Percentage overlap	Estimation accuracy		
		Average	Maximum	Minimum
5-15	22.86	95.51	99.16	86.28
15-20	37.24	93.33	98.68	85.31
20-25	43.48	92.72	98.18	83.18

control of the crystallization process. To see the effect of the number of processed images on the CSD estimation accuracy, a library of 500 particles was constructed and assumed to exist inside the crystallizer. From this library, a set of 50 images in which 0 to 20 particles exist were generated stochastically imitating the images captured by a camera during a crystallization process. By applying the algorithm developed in this work on these images, a crystal size distribution was constructed. This crystal size distribution was compared with the distribution of the actual library used to generate the images. This is shown in Fig. 4.9 from where it can be seen that the estimated frequency distribution (estimated CSD) is very similar to the true CSD represented by the library data. Similarly, this method was tested by increasing the number of images captured to 100. Comparison of the estimated CSD with the actual distribution for the 100 images (first set) is shown in Fig. 4.10. The experiment was repeated by changing the number of images to 25 and 500, to study the effect of number of images.

Each experimental run was repeated 25 times. The statistics of the distributions are computed and the results are compiled in Table 4.3. The mean of the actual library of particles is 100.52 (in pixel). The mean of distributions from the different "experiments" are compared in the second column of the Table 4.3. As the number of images is increased, the mean of the distribution approaches the "true" mean of the library. The variance of the distributions also behave in the same way. From Figures 4.9 and 4.10, it is noted that as we increase the number of images, the

actual distribution which exists within the crystallizer is estimated more accurately from the PVM images by the MOO based technique. It can also be seen there is no significant improvement in the accuracy when one increases the number of images from 100 to 500. From the fourth column of Table 4.3, it can be seen that the skewness of the actual and estimated distributions are close to 0, indicating a symmetric distribution. Similarly the kurtosis values are also close to each other and around 3 which denotes a normal distribution. Hence, by capturing an optimal number of images, the CSD can be estimated from the PVM images.

The effect of adding broken particles and small chips are compared by keeping the number of images constant at 100. Each experimental run is repeated 10 times. The results are shown in Table 4.4. By comparing the statistics in Table 4.4, it is evident that our algorithm does not have trouble in estimating CSD from PVM images with disturbances such as broken crystals and small particles. Therefore, this methodology can be applied to images from the crystallization process for estimating CSD in order to better control the crystallization process.

Table 4.3
Statistical mean measures obtained for the different "experimental" runs

Set Description	Mean	Variance	Skewness	Kurtosis
Actual	100.52	377.85	0.002	2.86
25 Images	101.79	382.16	-0.026	2.81
50 Images	100.84	382.56	-0.01	2.86
100 Images	100.68	372.53	-0.006	2.88
500 Images	100.56	375.72	-0.002	2.85

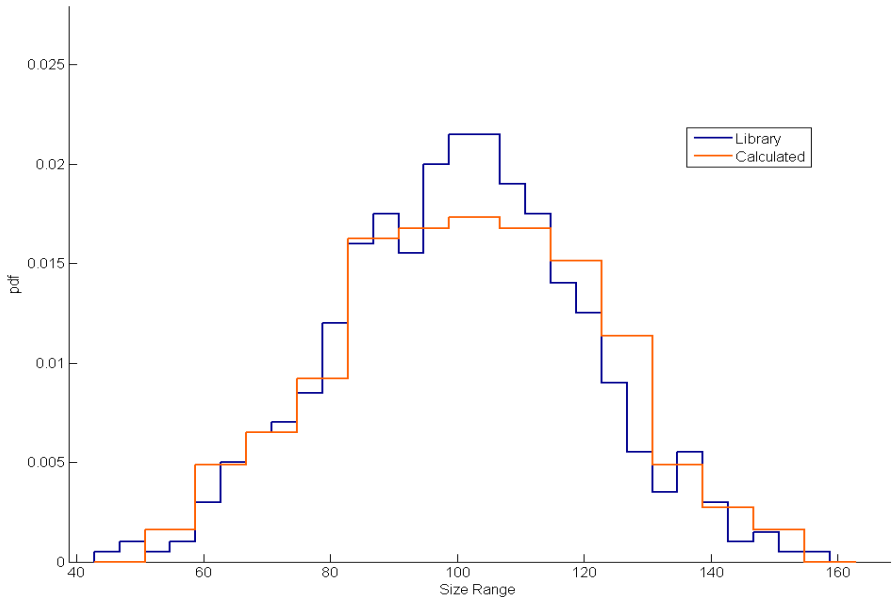

Fig. 4.9. Estimated CSD compared with actual CSD (50 Images)

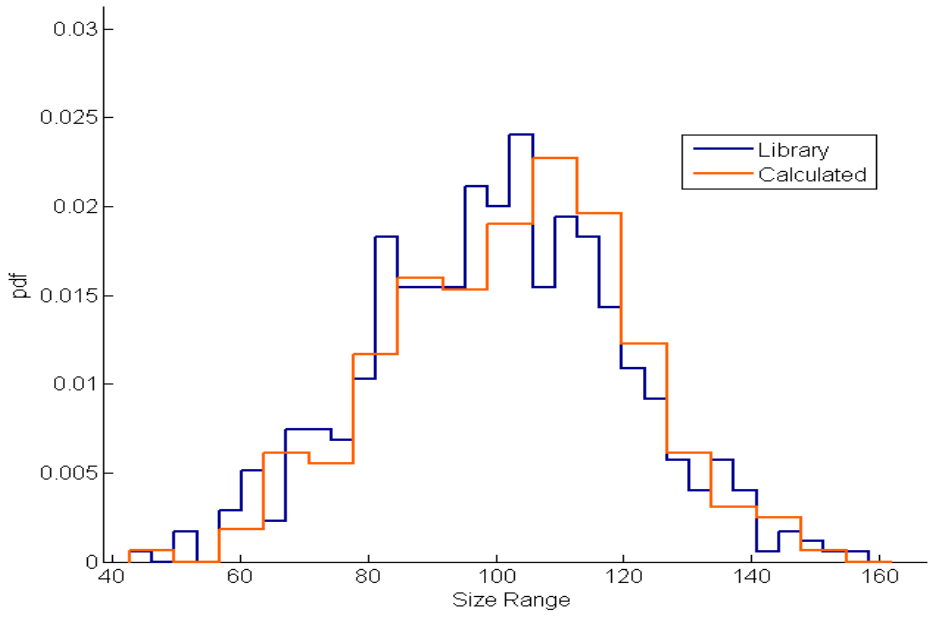

Fig. 4.10. Estimated CSD compared with actual CSD (100 Images)

Table 4.4
Statistical mean measures obtained for the different "experimental" runs of 100 images

Set Description	Mean	Variance	Skewness	Kurtosis
Normal	100.68	372.53	-0.006	2.88
Broken Crystals	100.84	380.24	0.01	2.85
Small Particles	100.42	381.4	-0.008	2.87

4.2 Case II - Classification of ultrasound breast cancer tumor images based on image analysis

A general introduction to this problem has been given in Section 2.6. In this section, the results obtained by the application of image analysis on the ultrasound images are discussed.

4.2.1 Image acquisition

A set of 30 ultrasound images of 10 breast cancer patients were obtained from International Islamic University Malaysia (IIUM) Breast Centre. Out of the 10 patients, 4 patients have cancer. The images used in this work were obtained in the *dicom* format. An example image is shown in Fig. 4.11. The details of the patient have been removed for confidentiality reasons.

4.2.2 Image pre-processing

Generally, ultrasound images are subjected to speckle reduction (noise removal) and image enhancement. Similar to what was done for crystallization images, speckle reduction was carried out with the help of median filtering. Image enhancement was carried out using the histogram equalization method.

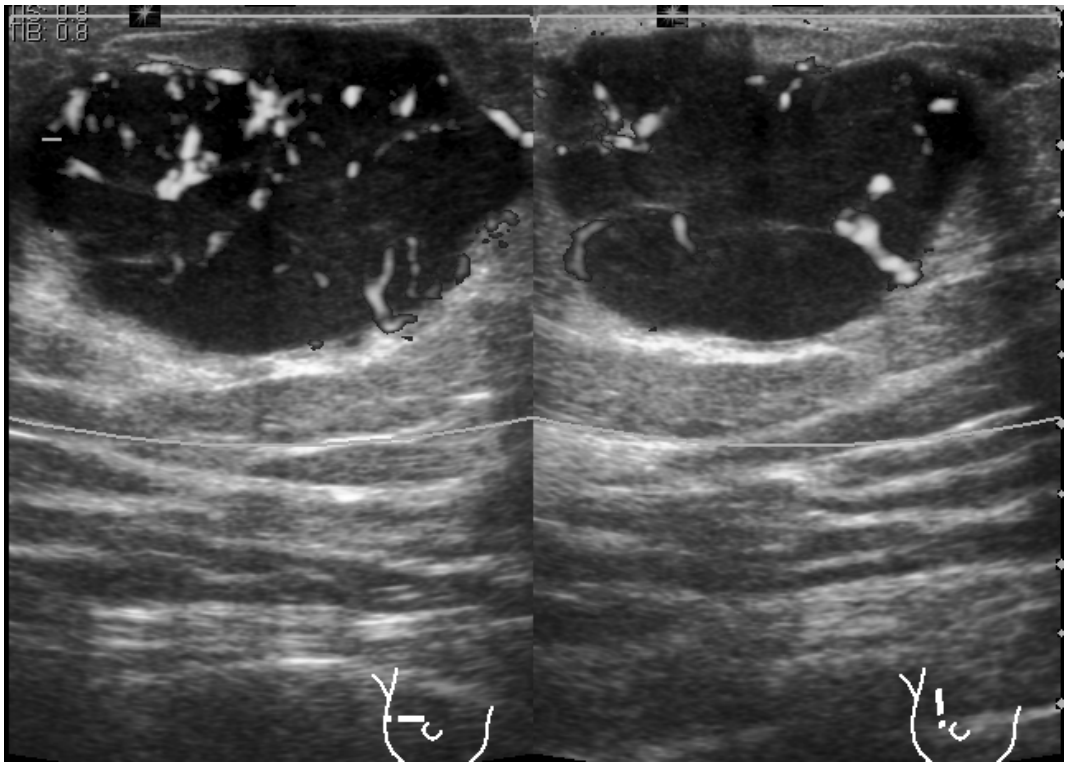

Fig. 4.11. Ultrasound image of breast tumor

4.2.3 Image segmentation

In this section, image segmentation is carried out by the MOO based image thresholding approach explained in Chapter 3. After segmentation, morphological operations are applied on the binary image to remove trivial objects and segments touching the border. The Pareto front is obtained and shown in Fig. 4.12. The optimal threshold is computed from the Pareto using the L_2-norm method. The original image is shown in Fig. 4.13(a). The images obtained after thresholding using the three considered methods (Otsu, minimum error and MOO based approach) are shown in Fig. 4.13(b), (c) and (d) respectively. The results show that Otsu method based thresholding identifies the tumor along with some dark regions and fails to differentiate between the particle boundary and some dark regions of the background, while minimum error based thresholding misses out major part of the tumor. From Fig. 4.13(d), it can be seen that MOO based thresholding performs

better than the other two methods. This segmentation accuracy in this image was evaluated by manually segmenting the tumor and calculating the misclassification rate. The misclassification rates of the tumors visible in the ultrasound image is calculated and shown in Table 4.5. From Fig. 4.13 and Table 4.5, it is very clear that MOO based approach segments the tumor better than the other two methods.

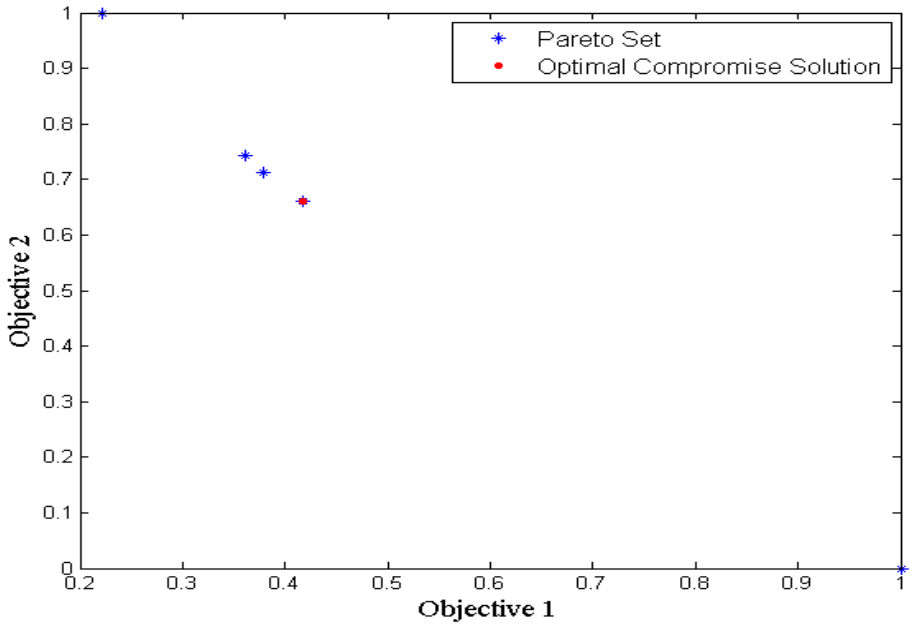

Fig. 4.12. Pareto plot - Breast image (ultrasound)

Table 4.5
Misclassification rate for breast ultrasound images

Example	Otsu Method	Minimum Error Method	MOO based segmentation
Tumor 1	42.83	22.16	10.43
Tumor 2	52.68	23.78	15.19

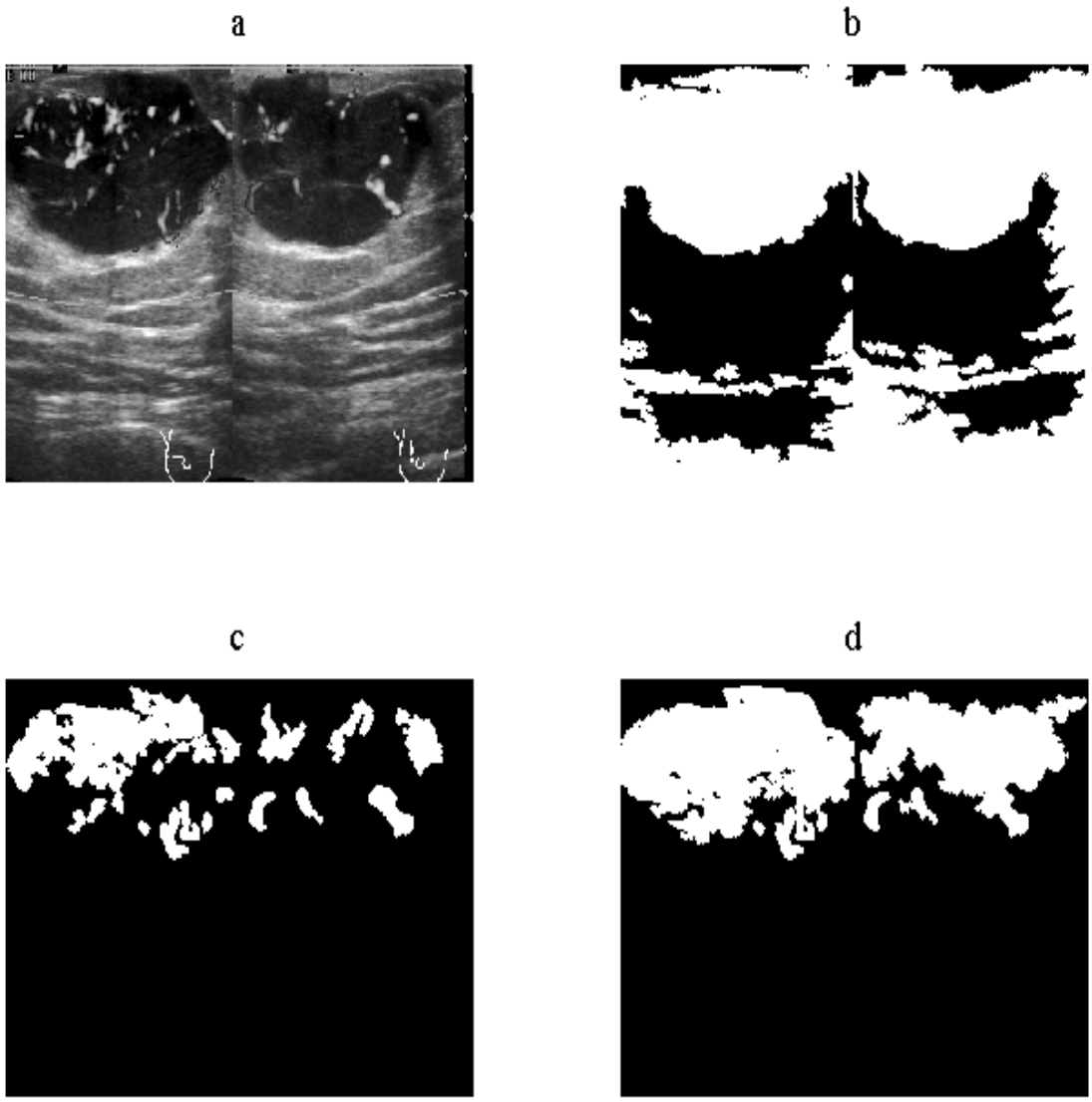

Fig. 4.13. (a) - Original image (b), (c), (d) Image after thresholding using Otsu method, Minimum error method, and MOO based segmentation respectively

4.2.4 Feature extraction

After segmenting the tumor from breast ultrasound image, the tumor segments can be characterized using feature extraction technique. The features that can be extracted from the tumor can be broadly classified into four major categories: texture, morphologic, model-based and descriptor features. In our algorithm, features

such as mean and variance of the intensity of the tumor area, the tumor area, the circumference of the tumor were estimated. The statistics obtained can be used to calculate the compactness of the tumor, aspect ratio, homogeneity of the region, etc. The features that were computed from the example image in this work are shown in Table 4.6.

Table 4.6
Extracted features of breast cancer tumors

Example	Area	Circumference	Compactness	Extent	Aspect Ratio
Tumor 1	43119	1269	0.3367	0.6708	1.6231
Tumor 2	37223.375	2004.5	0.116	0.7059	2.103

Based on features like those extracted in Table 4.6, breast cancer images can be classified into benign and malignant with the help of a classification tool (Cheng et al. 2010). The set of rules followed to classify the tumor vary between physicians. Based on the radiologist's requirements, extra features which are essential for classification can be also extracted. Hence, this algorithm can be useful in assisting radiologists to extract the features required for classification.

Chapter 5

CONCLUSIONS AND FUTURE WORK

5.1 Conclusions

As illustrated in this thesis, MOO based approach works better than current single objective based thresholding strategies. The MOO based approach gives a user an extra option for better thresholding. Segmentation is very important because the extracted region of interest will be further processed by other image analysis steps and the overall results will be affected by the quality of the results obtained at this step.

The estimation of CSD via image analysis is important for effective control of crystallization processes. The accuracy of the image analysis results largely depends on the image analysis methodologies chosen for the various image processing steps. Image segmentation is a key step in the overall image analysis procedure. Image thresholding by traditional methods fails if the image is noisy even after image preprocessing. However, the limitations of the traditional methods can be overcome using MOO based thresholding approach as is shown in this work. Using feature extraction techniques such as blob analysis, and minimum area enclosing rectangle, the CSD can be estimated. The results from this investigation show that the proposed algorithm has high estimation accuracy owing to its MOO based thresholding approach. This technique, therefore, offers an opportunity for automated control of crystallization processes leading to improved product quality. Image analysis techniques can also be extended in the case of other particulate process involved in the pharmaceutical, chemical and food industry.

Early detection of breast cancer can help in treating the disease much more effectively. Detection techniques must be accurate to prevent unwanted biopsies. Ultrasound imaging of breast tumors are preferred over mammography techniques due to lower rate of false positives. The classification of tumors varies largely due to high inter observer inconsistencies. In this work, image analysis technique based MOO approach was shown to allow segmentation of the tumor and determine its properties such as size, shape, etc. Hence, this algorithm can act as a tool in assisting radiologist for classification of benign masses from malignant.

5.2 Future work

On the average, it was found that the proposed MOO based method has an estimation accuracy greater than 92% when 20-25 particles exist in the image. However, this method does not estimate the size of overlapping particles. Therefore, if the size of the overlapped particles can be characterized, the number of images required to obtain the CSD can be reduced to bring down operation costs.

Therefore, the overlaps have to be handled during the processing of individual images. Overlapping particles need to be identified first. This can be done by using minimum area rectangle method. Firstly, the minimum area enclosing rectangle is calculated for the overlapping particle and compared with the actual area of the particle occupying the image obtained from blob analysis. Based on a small error criterion between the two areas, the blobs can be classified into overlaps and individual particles. After this step, there are two possible plans for identifying them as separate particles. The first approach is to classify each pixel in this overlapped region by assigning the pixel a label based on a set of rules. The second approach is to use model based segmentation, where models of particles can be fitted to separate touching and overlapping particles.

Different sets of features can be extracted from the breast tumor images. The current algorithm can be extended as a complete automated diagnosis and detection

tool by adding a suitable classification criterion made in consultation with a medical expert. Once a set of rules are decided, there are many classification tools for differentiating breast tumors.

REFERENCES

Bebis, G. (2004*a*), 'The geometry of perspective projection'.
URL: *http://www.cse.unr.edu/ bebis/CS791E/Notes/PerspectiveProjection.pdf*

Bebis, G. (2004*b*), 'Image operations'.
URL: *http://www.cse.unr.edu/ bebis/CS791E/Notes/PointProcess.pdf*

Bebis, G. (2004*c*), 'Thresholding'.
URL: *http://www.cse.unr.edu/ bebis/CS791E/Notes/Thresholding.pdf*

Bhanu, B., Lee, S. & Das, S. (1995), 'Adaptive image segmentation using genetic and hybrid search methods', *IEEE Transactions on Aerospace and Electronic Systems* **31**(4), 1268–1291.

Boncelet, C. (2005), Image noise models, *in* A. Bovik, ed., 'Handbook of Image and Video Processing (Second Edition)', Academic Press, Burlington, pp. 397–409.

Braatz, R. D. (2002), 'Advanced control of crystallization processes', *Annual Reviews in Control* **26**(1), 87–99.

Chang, R.-F., Wu, W.-J., Moon, W. K. & Chen, D.-R. (2005), 'Automatic ultrasound segmentation and morphology based diagnosis of solid breast tumors', *Breast Cancer Research and Treatment* **89**, 179–185.

Chen, D. R. Chang, R. F. H. Y. L. (1999), 'Computer-aided diagnosis applied to us of solid breast nodules by using neural networks', *Radiology* **213**, 407–412.

Cheng, H., Shan, J., Ju, W., Guo, Y. & Zhang, L. (2010), 'Automated breast cancer detection and classification using ultrasound images: A survey', *Pattern Recognition* **43**(1), 299–317.

Choraś, R. S. (2007), 'Image feature extraction techniques and their applications for cbir and biometrics systems', *International Journal of Biology and Biomedical Engineering* **1**, 6–16.

Dhawan, A. P. (2011), *Medical image analysis*, John Wiley & Sons, Inc., New Jersey.

Dougherty, G. (2009), *Digital image processing for medical applications*, Cambridge University Press, Cambridge, UK.

Dowsland, K. A. (1993), Simulated annealing, *in* 'Modern heuristic techniques for combinatorial problems', John Wiley & Sons, Inc., pp. 20–69.

Fisher, R. (1997), *Hypermedia Image Processing Reference*, Wiley, New York.

Fordham, S. D. (1977), 'Limitations of mammography', *International Surgery* **62**, 138–139.

Gino, M. C. (2004), 'Noise, noise, noise'.
URL: *http://www.astrophys-assist.com/educate/noise/noise.htm*

Glasbey, C. (1993), 'An analysis of histogram-based thresholding algorithms', *CVGIP: Graphical Models and Image Processing* **55**(6), 532–537.

Gonzalez, R. C. & Woods, R. E. (2008), *Digital image processing*, Pearson Education, Upper Saddle River, New Jersey.

Gonzalez, R., Woods, R. & Eddins, S. (2011), *Digital Image Processing Using MATLAB, 2nd ed.*, Gatesmark Publishing.

Hadjiiski, L., Sahiner, B. & Chan, H. P. (2006), 'Advances in computer-aided diagnosis for breast cancer', *Current Opinion in Obstetrics & Gynecology* **18**, 64–70.

Haralick, R. M., Shanmugam, K. & Dinstein, I. (1973), 'Textural features for image classification', *IEEE Transactions on Systems, Man and Cybernetics* **3**(6), 610–621.

Horsch, K., Giger, M. L., Venta, L. A. & Vyborny, C. J. (2001), 'Automatic segmentation of breast lesions on ultrasound', *Medical Physics* **28**(8), 1652–1659.

Instruments, N. (2008), 'Image analysis and processing'.
URL: *http://zone.ni.com/devzone/cda/tut/p/id/3470#toc2*

Jain, A. K. (2001), *Fundamentals of digital image processing*, Prentice-Hall, Inc., Englewood Cliffs, New Jersey.

Jain, A. K., Duin, R. P. W. & Mao, J. (2000), 'Statistical pattern recognition: A review', *IEEE Transactions on Pattern Analysis and Machine Intelligence* **22**(1), 4–37.

Jemal, A., Bray, F., Center, M. M., Ferlay, J., Ward, E. & Forman, D. (2011), 'Global cancer statistics', *CA: A Cancer Journal for Clinicians* **61**(2), 69–90.

Joo, S., Moon, W. K. & Kim, H. C. (2004), Computer-aided diagnosis of solid breast nodules on ultrasound with digital image processing and artificial neural network, *in* 'Engineering in Medicine and Biology Society, 2004. IEMBS '04. 26th Annual International Conference of the IEEE', Vol. 1, pp. 1397–1400.

Joo, S., Yang, Y. S., Moon, W. K. & Kim, H. C. (2004), 'Computer-aided diagnosis of solid breast nodules: use of an artificial neural network based on multiple sonographic features', *IEEE Transactions on Medical Imaging* **23**(10), 1292–1300.

Kapur, J., Sahoo, P. & Wong, A. (1985), 'A new method for gray-level picture thresholding using the entropy of the histogram', *Computer Vision, Graphics, and Image Processing* **29**(3), 273–285.

Kasprzak, E. & Lewis, K. (2001), 'Pareto analysis in multiobjective optimization using the collinearity theorem and scaling method', *Structural and Multidisciplinary Optimization* **22**(3), 208–218.

Kirkpatrick, S., Gelatt, C. D. & Vecchi, M. P. (1983), 'Optimization by simulated annealing', *Science* **220**(4598), 671–680.

Kittler, J. & Illingworth, J. (1986), 'Minimum error thresholding', *Pattern Recognition* **19**(1), 41–47.

Korath, J. M., Abbas, A. & Romagnoli, J. A. (2006), Monitoring of crystallization processes: a novel approach for the separation of touching edges in crystal particle images, *in* 'In proceedings of AIChE'.

Korath, J. M., Abbas, A. & Romagnoli, J. A. (2007), 'Separating touching and overlapping objects in particle images - a combined approach', *Chemical Engineering Transactions* **11**, 167–172.

Larsen, P. A. & Rawlings, J. B. (2008), 'Assessing the reliability of particle number density measurements obtained by image analysis', *Particle & Particle Systems Characterization* **25**(5-6), 420–433.

Larsen, P., Patience, D. & Rawlings, J. (2006), 'Industrial crystallization process control', *Control Systems, IEEE* **26**(4), 70–80.

Larsen, P., Rawlings, J. & Ferrier, N. (2006), 'An algorithm for analyzing noisy, in situ images of high-aspect-ratio crystals to monitor particle size distribution', *Chemical Engineering Science* **61**(16), 5236–5248.

Larsen, P., Rawlings, J. & Ferrier, N. (2007), 'Model-based object recognition to measure crystal size and shape distributions from in situ video images', *Chemical Engineering Science* **62**(5), 1430–1441.

Lovette, M. A., Browning, A. R., Griffin, D. W., Sizemore, J. P., Snyder, R. C. & Doherty, M. F. (2008), 'Crystal shape engineering', *Industrial & Engineering Chemistry Research* **47**(24), 9812–9833.

Metropolis, N., Rosenbluth, A., Rosenbluth, M., Teller, A. & Teller, E. (1953), 'Equation of state calculations by fast computing machines', *The Journal of Chemical Physics* **21**(6), 1087–1092.

Miettinen, K. (1999), *Nonlinear multiobjective optimization*, Kluwer Academic Publishers, Boston.

Miettinen, K. & Hakanen, J. (2009), *Multi-objective optimization techniques and applications in chemical engineering*, World Scientific Publishing, chapter Why Use Interactive Multi-Objective Optimization in Chemical Process Design?, pp. 153–188.

Mironescu, I. D. & Mironescu, V. (2006), 'Image analysis for crystallization process control', *Journal of Agroalimentary Processes and Technologies* **XII**, 7–12.

Monnier, O., Fevotte, G., Hoff, C. & Klein, J. (1997), 'Model identification of batch cooling crystallizations through calorimetry and image analysis', *Chemical Engineering Science* **52**(7), 1125–1139.

Moon, W. K., Chang, R.-F., Chen, C.-J., Chen, D.-R. & Chen, W.-L. (2005), 'Solid breast masses: Classification with computer-aided analysis of continuous us images obtained with probe compression', *Radiology* **236**(2), 458–464.

Nagabhushana, S. (2006), *Computer Vision And Image Processing*, New Age International.

Nakib, A., Oulhadj, H. & Siarry, P. (2007), 'Image histogram thresholding based on multiobjective optimization', *Signal Processing* **87**(11), 2516–2534.

Nakib, A., Oulhadj, H. & Siarry, P. (2008), 'Non-supervised image segmentation based on multiobjective optimization', *Pattern Recognition Letters* **29**(2), 161–172.

Nakib, A., Oulhadj, H. & Siarry, P. (2009*a*), 'Fractional differentiation and non-pareto multiobjective optimization for image thresholding', *Engineering Applications of Artificial Intelligence* **22**(2), 236–249.

Nakib, A., Oulhadj, H. & Siarry, P. (2009*b*), 'A thresholding method based on two-dimensional fractional differentiation', *Image and Vision Computing* **27**(9), 1343–1357.

Nakib, A., Oulhadj, H. & Siarry, P. (2010), 'Image thresholding based on pareto multiobjective optimization', *Engineering Applications of Artificial Intelligence* **23**(3), 313–320.

Niuniu, X. & Yuxun, L. (2010), Review of decision trees, *in* 'Computer Science and Information Technology (ICCSIT), 2010 3rd IEEE International Conference', Vol. 5, pp. 105–109.

Otsu, N. (1979), 'A threshold selection method from gray-level histograms', *IEEE Transactions on Systems, Man and Cybernetics* **9**(1), 62–66.

Oullion, M., Puel, F., Févotte, G., Righini, S. & Carvin, P. (2007), 'Industrial batch crystallization of a plate-like organic product. in situ monitoring and 2d-csd modelling. part 1: Experimental study', *Chemical Engineering Science* **62**(3), 820–832.

Patience, D. B. & Rawlings, J. B. (2001), 'Particle-shape monitoring and control in crystallization processes', *AIChE J.* **47**(9), 2125–2130.

Plummer, C. J. G. & Kausch, H. H. (1995), 'Real-time image analysis and numerical simulation of isothermal spherulite nucleation and growth in polyoxymethylene', *Colloid and Polymer Science* **273**, 719–732.

Pons, M.-N. & Vivier, H. (1990), 'Crystallization monitoring by quantitative image analysis', *Analytica Chimica Acta* **238**, 243–249.

Presles, B., Debayle, J., Févotte, G. & Pinoli, J.-C. (2010), 'Novel image analysis method for in situ monitoring the particle size distribution of batch crystallization processes', *Journal of Electronic Imaging* **19**(3), 031207.

Prewitt, J. M. S. & Mendelsohn, M. L. (1966), 'The analysis of cell images', *Annals of the New York Academy of Sciences* **128**(3), 1035–1053.

Puel, F., Féotte, G. & Klein, J. (2003), 'Simulation and analysis of industrial crystallization processes through multidimensional population balance equations. part 2: a study of semi-batch crystallization', *Chemical Engineering Science* **58**(16), 3729–3740.

Puel, F., Marchal, P. & Klein, J. (1997), 'Habit transient analysis in industrial crystallization using two dimensional crystal sizing technique', *Chemical Engineering Research and Design* **75**(2), 193–205.

Pun, T. (1980), 'A new method for grey-level picture thresholding using the entropy of the histogram', *Signal Processing* **2**(3), 223–237.

Rangaiah, G. P. (2009), *Multi-objective optimization techniques and applications in chemical engineering*, World Scientific Publishing, Singapore.

Sahoo, P. K., Soltani, S., Wong, A. K. & Chen, Y. C. (1988), 'A survey of thresholding techniques', *Computer Vision, Graphics, and Image Processing* **41**(2), 233–260.

Sezgin, M. & Sankur, B. (2004), 'Survey over image thresholding techniques and quantitative performance evaluation', *Journal of Electronic Imaging* **13**(1), 146–168.

Smith, S. W. (1997), *The Scientist and Engineer's Guide to Digital Signal Processing*, California Technical Publishing.

Song, J. H., Venkatesh, S. S., Conant, E. A., Arger, P. H. & Sehgal, C. M. (2005), 'Comparative analysis of logistic regression and artificial neural network for computer-aided diagnosis of breast masses', *Academic Radiology* **12**(4), 487–495.

Srinivas, N. & Deb, K. (1994), 'Multiobjective optimization using nondominated sorting in genetic algorithms', *Evolutionary Computation* **2**, 221–248.

Steger, C., Ulrich, M. & Weidemann, C. (2008), *Machine vision algorithms and applications*, Wiley-VCH, Weinheim.

Tamaki, H., Kita, H. & Kobayashi, S. (1996), Multi-objective optimization by genetic algorithms: a review, *in* 'Evolutionary Computation, 1996., Proceedings of IEEE International Conference', pp. 517–522.

Toussaint, G. (1983), Solving geometric problems with the rotating calipers, *in* 'Proceedings of IEEE Mediterranean Electrotechnical Conference', pp. 1–8.

Černý, V. (1985), 'Thermodynamical approach to the traveling salesman problem: An efficient simulation algorithm', *Journal of Optimization Theory and Applications* **45**(1), 41–51.

Young, I., Gerbrands, J. & Van Vliet, L. (1995), *Fundamentals of image processing*, TUDelft, Faculty of Applied Physics, Pattern Recognition Group.

Zhang, X. & Liu, C. (2009), A two-dimensional image thresholding method based on multiobjective optimization, *in* 'Computer Network and Multimedia Technology, 2009. CNMT 2009. International Symposium', pp. 1–5.

Zhou, Y., Doan, X.-T. & Srinivasan, R. (2006), Real-time imaging and product quality characterization for control of particulate processes, *in* W. Marquardt & C. Pantelides, eds, '16th European Symposium on Computer Aided Process Engineering and 9th International Symposium on Process Systems Engineering', Vol. Volume 21, Elsevier, pp. 775–780.

Zhou, Y., Srinivasan, R. & Lakshminarayanan, S. (2009), 'Critical evaluation of image processing approaches for real-time crystal size measurements', *Computers and Chemical Engineering* **33**(5), 1022–1035.

Appendix
Publications & Presentations

Book Chapter

- Karthik Raja Periasamy and S. Lakshminarayanan, *Multi-Objective Optimization: Developments and Prospects for Chemical Engineering*, John Wiley & Sons, Chapter: Estimation of Crystal Size Distribution: Image thresholding based on Multi-Objective Optimization. (Under Review)

Poster Presentation

- Karthik Raja Periasamy and S. Lakshminarayanan, Applying Image Analysis to control quality of pharmaceutical products, In *ISPE Conference 2011*, Singapore, 2011.

Proceedings

- Karthik Raja Periasamy, Kanchi Lakshmi Kiran, S.C. Humairah Abdul, D.P. Perumal, Balu Ranganathan and S. Lakshminarayanan, Computer-Aided Diagnosis of Breast Cancer using Ultrasound Images, In *proceedings of* 1^{st} *SHBC 2010*, Singapore, 2010.